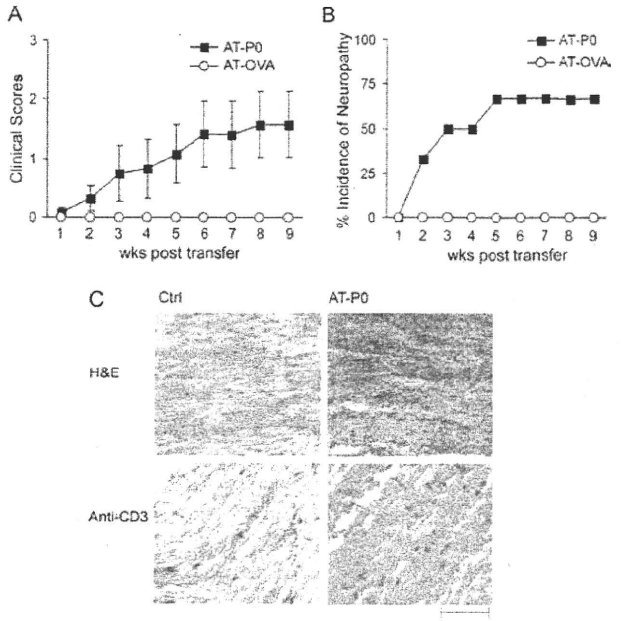

FIGURE 5. Adoptive transfer (AT) of P0 (180–199)-specific and OVA-reactive $CD4^+$ T cell lines into 8- to 10-wk-old female NOD.SCID mice. *A*, Summary of clinical scores ($n = 6$ for AT-P0; $n = 3$ for AT-OVA). P0-specific T cell lines were generated from SAP mice, whereas OVA-specific T cells lines were generated from WT NOD mice immunized with OVA. *B*, Incidence of neuropathy in AT-P0 mice and AT-OVA mice. *C*, Histologic examples of sciatic nerve sections showing T cell infiltrates ($CD3^+$ cells) in nerves from AT-P0 mice. Hematoxylin was used for counterstaining in immunohistochemical studies. Scale bar represents 100 μm for H&E and 50 μm for anti-CD3.

$CD4^+$ T cells but not sera from SAP mice are sufficient to transfer disease to NOD.SCID mice (3). To further examine whether P0-reactive T cells are pathogenic in SAP, we generated P0-reactive T cell lines from pooled splenocytes and lymph node cells isolated from inguinal and axillary lymph nodes of SAP mice (7- to 8-mo-old). These cell lines secrete greater amounts of IFN-γ (14.7–15.4 ng/ml) than IL-17 (0.5–0.67 ng/ml) upon exposure to P0 (180–199), but only IFN-γ secretion was inhibited by Ab α MHC class II (I-A/I-E) (10 μg/ml) (data not shown). Adoptive transfer of 6.5×10^6 P0-reactive $CD4^+$ T cell lines (AT-P0) led to the development of peripheral neuropathy in four of six (66.7%) NOD.SCID mice, as shown in Fig. 5, *A* and *B*. By comparison, transfer of purified $CD4^+$ T cells from WT NOD mice or OVA-reactive T cell lines (AT-OVA) did not induce neuropathy ($n = 3$ each). Because we were not able to generate OVA-specific T cell lines from SAP mice, these cell lines were derived from WT NOD mice immunized with OVA. Results were confirmed with grip strength measurements at peak disease or at the end of 9 wk. Forelimb grip strength (in Newtons) was 2.37 ± 0.26 and 3.2 ± 0.01 in AT-P0 and AT-OVA mice, respectively ($p < 0.01$), whereas hindlimb grip strength was 0.38 ± 0.11, and 1.02 ± 0.01, respectively ($p < 0.0003$) (data not shown). Histologic studies revealed the presence of T cell infiltrates in sciatic nerves of symptomatic AT-P0 mice (Fig. 5*C*).

Lastly, we investigated whether SAP can be prevented in B7-2 KO NOD mice by a single i.v. injection of 200 μg P0 (180–199) at 2–4 mo of age. As depicted in Fig. 6, *A* and *B*, a very mild neuropathy was observed at 8 mo in only two of nine (22.2%) B7-2 KO mice injected with P0 (180–199), as compared with a more severe neuropathy in 10/10 (100%) mice receiving PBS, and in 5/6 (83.3%) animals given other peptides (OVA (323–339) or P2 (53–78)). In P0-injected mice, there was no decline in grip strength over time, in contrast to grip strength measurements in other groups of animals (Fig. 6*C*). Furthermore, sciatic nerve conduction studies revealed a significant difference in distal latency, conduction velocity and amplitude of the motor response in P0-injected mice compared with those from other groups of animals (Fig. 6*D*). No improvement in clinical severity was observed when P0 (180–199) was given at 8 mo (after disease onset) ($n = 2$, data not shown). Immunologic studies done at 8 mo revealed that there was a significant attenuation of the proliferative response to P0 (180–199), and a decline in IL-2 and IFN-γ secretion in splenocytes from animals injected with P0 at 2–4 mo. No significant effect on IL-10 or IL-17 levels was noted (Fig. 7). Taken together, these

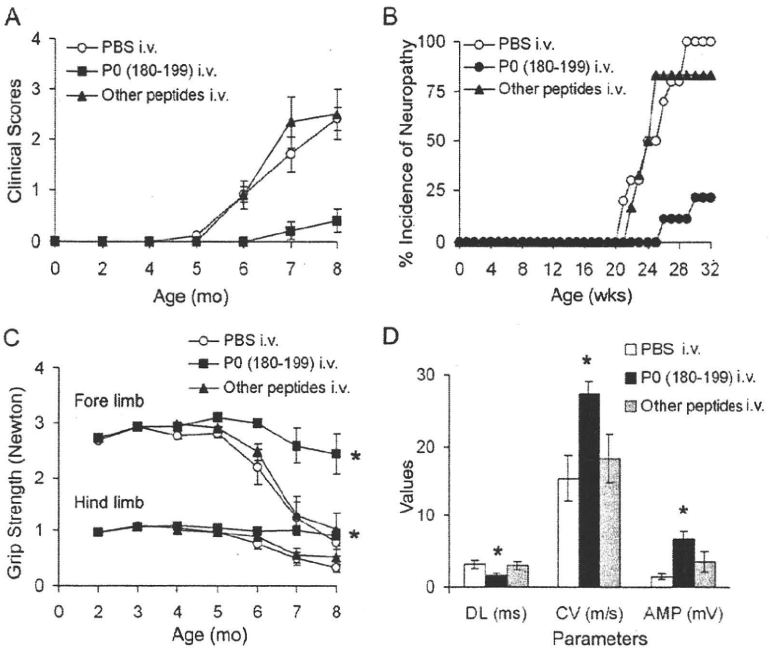

FIGURE 6. Prevention of SAP by a single i.v. injection of P0 (180–199), but not by injection of PBS or other peptides in B7-2 KO NOD mice at 2 or 4 mo. *A*, Clinical scores. Three groups of animals were compared ($n = 9$ for P0 (180–199), $n = 10$ for PBS, $n = 3$ each for other peptides including P2 (53–78) and OVA (323–339)). $p < 0.0001$ for P0 (180–199) vs PBS or other peptides at 8 mo. Peptide dose injected was 200 μg. *B*, Incidence of neuropathy in these three groups of mice. *C*, Grip strength measurements. *, $p < 0.0006$ for P0 (180–199) vs PBS and other peptides in forelimb at 8 mo, and *, $p < 0.0001$ in hindlimb grip strength. *D*, Sciatic nerve electrophysiology at 8 mo. Distal latency (DL), conduction velocity (CV), and amplitude (AMP) of sciatic motor responses were measured. *, $p < 0.009$ in distal latency measure for P0 (180–199) vs PBS or other peptides; *, $p < 0.003$ in conduction velocity; *, $p < 0.001$ in amplitude measure.

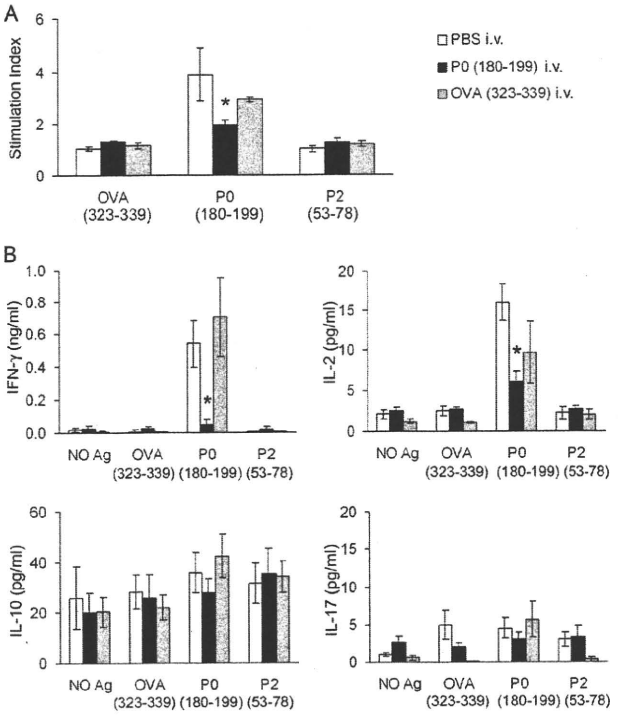

FIGURE 7. Suppression of splenocyte proliferation and Th1 cytokine secretion in B7-2 KO NOD mice given i.v. injection of P0 (180–199) at 2 or 4 mo. Three groups of mice were sacrificed at 8 mo (PBS group, $n = 4$; P0 group, $n = 6$; OVA group, $n = 3$). *A*, Proliferative responses of splenocytes to 20 μg/ml OVA (323–339), P0 (180–199), and P2 (53–78). Treatment duration was 72 h. The proliferative response to P0 (180–199) was decreased in splenocytes from P0-tolerized animals. *, $p < 0.004$ for P0 vs PBS group, and *, $p < 0.008$ for P0 vs OVA group). *B*, Cytokine responses of splenocytes to the same Ags in replicate cultures. Treatment duration was 48 h. *, $p < 0.03$ for P0 vs PBS group and $p < 0.003$ for P0 vs OVA group for IFN-γ; *, $p < 0.002$ for P0 vs PBS group for IL-2, but $p > 0.05$ for P0 vs OVA group. There was no significant difference in IL-10 and IL-17 production in response to P0 (180–199) among three groups of animals.

results indicate that myelin P0 (180–199) is one of the autoantigens involved in the development of SAP.

Discussion

NOD mice exhibit a number of immune system defects that contribute to their susceptibility to develop multiorgan autoimmunity (1). Similar to other models of autoimmunity, functional polarization of Th subsets is one of the crucial factors in the pathogenesis of type 1 diabetes. Th1 effector response (high IFN-γ to IL-4 ratio) is associated with destructive insulitis, although a dual pathogenic and protective role for IFN-γ has been demonstrated by other investigators (28–31). Recently, evidence has been introduced to indicate that IL-17 may contribute to the development of type 1 diabetes (31, 32).

We observed changes in cytokine and chemokine microenvironment in the spleens of B7-2 KO NOD mice, with IL-17 and IFN-γ predominating during the preclinical phase and clinical phase, respectively. That IFN-γ is a key effector mediating nerve damage in SAP mice is supported by the following: 1) IFN-γ and not IL-17 transcripts predominate in sciatic nerves of symptomatic mice, 2) splenocytes from symptomatic mice produce IFN-γ and not IL-17 upon stimulation with P0 (180–199); and 3) there was an increase in IFN-γ-producing, but not in IL-17-producing $CD4^+$ T cells in spleens of SAP mice at 6–8 mo when compared with age-matched WT NOD mice. Furthermore, disease severity in both SAP and EAN is attenuated in mice deficient in IFN-γ or its receptor, respectively (33, 34). Although there is evidence supporting a Th1 bias in SAP, the role of Th17 cells and the source of increased IL-17 transcripts in spleens of 4–6 mo old B7-2 KO mice remain to be clarified. Both Th1 and Th17 cells have been implicated in experimental autoimmune encephalomyelitis, though recent data indicate that they induce distinct types of CNS inflammatory disease characterized by macrophage-rich infiltrates and neutrophil-rich infiltrates, respectively (8, 35–37). It has also been reported that increased Th17 to Th1 ratio is more critical in the induction of CNS inflammation than in spinal cord inflammation (38).

The decline in IL-10 expression in spleens and its absence in sciatic nerves may contribute to disease development and progression in SAP. IL-10 expression correlates with spontaneous recovery in EAN, and exogenous IL-10 suppresses EAN by down-regulating Th1 responses (39, 40). The role of TNF-α in inflammatory neuropathies is more complex, as both anti-inflammatory and proinflammatory actions of TNF-α have been reported (41, 42). With regards to chemokines, the transient dip in CCL2 transcript levels in spleens is interesting. CCL2 KO mice have diminished Th2 cytokines supporting a role for CCL2 in the regulation of Th2 polarization, in addition to its role as a monocyte chemoattractant (43). Cytokines and chemokines that are up-regulated in sciatic nerves of SAP mice are the same ones found in EAN and CIDP nerves with prominent increase in TNF-α, IFN-γ, CXCL10, and RANTES expression (10, 44–46).

Aside from cytokine perturbations, another crucial determinant in the development of autoimmune diseases is the delicate balance between autoreactive T cells and Tregs, which is controlled by B7-2 and other costimulatory molecules (4, 6, 47). Though both B7-1 and B7-2 bind to their receptors CD28 and CTLA-4, signaling through CD28 promotes T cell activation, whereas signaling through CTLA-4 down-regulates T cell responses (48, 49). $CD28^{-/-}$ C57BL/6 mice are resistant to EAN induction and CTLA-4 blockade enhances the severity of EAN (50, 51). The requirement for B7-1 vs B7-2 in autoimmunity is more complex and is influenced by genetic background, and the target organ involved. Absence of either B7-1 or B7-2 leads to attenuation of experimental autoimmune encephalomyelitis induced in NOD mice but not in C57BL/6 mice (52, 53). B7-2 elimination triggers the development of SAP in NOD mice but not in C57BL/6 mice. In SAP nerves, high levels of B7-1 expression were observed in infiltrating $CD11b^+$ and $CD11c^+$ cells (3). Similarly, there is a preferential up-regulation of B7-1 in CIDP nerves (54). Yet, neuropathy is accelerated by treatment with anti-B7-1 Ab in B7-2 KO NOD mice (6, 33). Collectively, these findings suggest a dominant role of B7-1 in the development of autoimmune neuropathies, but its requirement can be bypassed in the absence of functional Treg compartment. It is possible that other costimulatory molecules also play a role in inflammatory neuropathies. ICOS and its unique ligand (ICOS-L) mRNA are up-regulated in infiltrating T cells and macrophages, respectively, in nerve samples from CIDP and other inflammatory neuropathies (55). Other investigators found up-regulation of a costimulatory molecule in Schwann cells of CIDP nerves that was detected by anti-BB-1 Ab, but not by anti-B7-1 or anti-B7-2 Abs (56).

It is intriguing that elimination of a costimulatory molecule such as B7-2 would shift the autoimmunity from pancreatic islets to peripheral nervous tissue. Due to a generalized defect in central tolerance induction, NOD mice contain a diverse repertoire of T cells reactive against multiple tissue Ags including several nervous system Ags such as myelin basic protein and GFAP (26, 57). Yet, B7-2 KO NOD mice develop neuropathy spontaneously but not encephalomyelitis. Perhaps, the above dichotomy is partially due

to a lesser ability of the blood nerve barrier than the blood brain barrier to impede lymphocytes access to the tissues. A second explanation could be derived from our data. Splenocyte proliferative responses indicate that an autoantigen resides in peripheral myelin or myelinating Schwann cells. Further studies revealed that P0 (180–199) but not P0 (106–125) or P0 (41–60) elicited splenocyte proliferative and Th1 cytokine responses. Two P0 peptides used in the current study, P0 (180–199) and P0 (106–125), have been used to induce EAN in resistant C57BL/6 mice (34, 58, 59). Mice are generally more resistant to EAN induction than Lewis rats. The third peptide, P0 (41–60), has been reported to elicit a strong immune response in P0 KO mice but not in WT mice immunized with peripheral myelin (60). Interestingly, P0 is expressed by peri-islet Schwann cells, which would not be expected of typical nonmyelinating Schwann cells with rare exceptions such as perisynaptic Schwann cells (61). These findings imply that the initiation and amplification of autoreactivity to P0 can occur either in pancreatic islets or in peripheral nerves, and taken together with the imperfect blood nerve barrier, would account for the propensity of NOD mice to develop SAP rather than encephalomyelitis.

We found that P0 (180–199) reactive T cells are pathogenic, based on our data from adoptive transfer and i.v. P0 experiments. The i.v. injection of soluble proteins such as myelin basic protein induces tolerance in experimental autoimmune encephalomyelitis by clonal deletion, anergy or induction of Th2 Tregs depending on the timing of administration (62–64). The effect of soluble Ag treatment on effector T cell mobility and cytokine up-regulation can be extremely rapid (within minutes) associated with trapping of these cells within lymphoid organs and later activation-induced cell death (65). In our study, a single i.v. injection of P0 peptide at 2 or 4 mo was sufficient to prevent SAP, which was associated with decreased activation of Th1 cells in response to P0 but was not accompanied by a shift to Th2 polarization. That myelin P0 is one of the SAP Ags has been demonstrated recently by Bour-Jourdan and colleagues using a different approach. Oligoclonal Ab responses to a 30-kDa protein were detected in accelerated models of autoimmune neuropathy, and the targeted protein was subsequently identified as myelin P0 by mass spectrometry (66). We found that Ab responses to P0 are more frequent in 6- to 8-mo-old than in younger B7-2 KO NOD mice or WT NOD mice. Further studies are required to determine whether P0 Abs contribute to the pathogenesis of SAP, or simply act as markers of peripheral nerve damage.

That a CIDP-like illness can develop on a background of diabetes is interesting, given similar observations in humans; however, not all patients reported in the literature had type 1 diabetes (67–70). There are other findings demonstrating a link between islet and nervous system autoimmunity, or supporting a role of neurons and glial cells in type 1 diabetes. Islet inflammation and insulin resistance are controlled by $TRPV^+$ PNS (71). Furthermore, GFAP-reactive T cell lines can transfer insulitis to NOD. SCID mice (26). It would be interesting to determine whether induction of tolerance to P0 would lead to suppression of islet autoimmunity in future studies. It is also recognized that some islet autoantigens are constituents of the nervous system such as glutamic acid decarboxylases GAD65 and GAD67; Ab α glutamic acid decarboxylase is associated with specific neurologic syndromes such as stiff person syndrome (72).

In summary, we found that 1) elimination of B7-2 leads to altered cytokine and chemokine milieu in lymphoid organs; 2) SAP is primarily a Th1-mediated disease; the cytokine and chemokine profile mimics that observed in CIDP nerves; and 3) myelin P0 is one of the autoantigens in SAP. These findings do not exclude the possibility of intramolecular spreading involving other P0 epitopes, intermolecular spreading to other PNS Ags, or a possible role for autoantibodies/B cells in the progression of SAP. The expression of P0 by peri-islet Schwann cells provides a potential mechanism linking islet autoimmunity and inflammatory neuropathy.

Acknowledgments

We thank Dr. J. A. Bluestone for generously providing B7-$2^{-/-}$ NOD mice. We also thank Shawna Cook for maintenance of mouse colony, Dr. Y. X. Fu for helpful discussions, and Dr. Barry Arnason for critical review of the manuscript.

Disclosures

The authors have no financial conflict of interest.

References

1. Anderson, M. S., and J. A. Bluestone. 2005. The NOD mouse: a model of immune dysregulation. *Annu. Rev. Immunol.* 23: 447–485.
2. Lenschow, D. J., S. C. Ho, H. Sattar, L. Rhee, G. Gray, N. Nabavi, K. C. Herold, and J. A. Bluestone. 1995. Differential effects of anti-B7-1 and anti-B7-2 monoclonal antibody treatment on the development of diabetes in the nonobese diabetic mouse. *J. Exp. Med.* 181: 1145–1155.
3. Salomon, B., L. Rhee, H. Bour-Jordan, H. Hsin, A. Montag, B. Soliven, J. Arcella, A. M. Girvin, J. Padilla, S. D. Miller, and J. A. Bluestone. 2001. Development of spontaneous autoimmune peripheral polyneuropathy in B7-2-deficient NOD mice. *J. Exp. Med.* 194: 677–684.
4. Yadav, D., V. Judkowski, M. Flodstrom-Tullberg, L. Sterling, W. L. Redmond, L. Sherman, and N. Sarvetnick. 2004. B7-2 (CD86) controls the priming of autoreactive CD4 T cell response against pancreatic islets. *J. Immunol.* 173: 3631–3639.
5. Koller, H., B. C. Kieseier, S. Jander, and H. P. Hartung. 2005. Chronic inflammatory demyelinating polyneuropathy. *N. Engl. J. Med.* 352: 1343–1356.
6. Bour-Jordan, H., B. L. Salomon, H. L. Thompson, G. L. Szot, M. R. Bernhard, and J. A. Bluestone. 2004. Costimulation controls diabetes by altering the balance of pathogenic and regulatory T cells. *J. Clin. Invest.* 114: 979–987.
7. Mosmann, T. R., and R. L. Coffman. 1989. TH1 and TH2 cells: different patterns of lymphokine secretion lead to different functional properties. *Annu. Rev. Immunol.* 7: 145–173.
8. Langrish, C. L., Y. Chen, W. M. Blumenschein, J. Mattson, B. Basham, J. D. Sedgwick, T. McClanahan, R. A. Kastelein, and D. J. Cua. 2005. IL-23 drives a pathogenic T cell population that induces autoimmune inflammation. *J. Exp. Med.* 201: 233–240.
9. Bettelli, E., M. Oukka, and V. K. Kuchroo. 2007. T_H-17 cells in the circle of immunity and autoimmunity. *Nat. Immunol.* 8: 345–350.
10. Kieseier, B. C., M. Tani, D. Mahad, N. Oka, T. Ho, N. Woodroofe, J. W. Griffin, K. V. Toyka, R. M. Ransohoff, and H. P. Hartung. 2002. Chemokines and chemokine receptors in inflammatory demyelinating neuropathies: a central role for IP-10. *Brain* 125: 823–834.
11. Press, R., M. Pashenkov, J. P. Jin, and H. Link. 2003. Aberrated levels of cerebrospinal fluid chemokines in Guillain-Barré syndrome and chronic inflammatory demyelinating polyradiculoneuropathy. *J. Clin. Immunol.* 23: 259–267.
12. Brostoff, S. W., S. Levit, and J. M. Powers. 1977. Induction of experimental allergic neuritis with a peptide from myelin P2 basic protein. *Nature* 268: 752–753.
13. Milner, P., C. A. Lovelidge, W. A. Taylor, and R. A. Hughes. 1987. P0 myelin protein produces experimental allergic neuritis in Lewis rats. *J. Neurol. Sci.* 79: 275–285.
14. Hahn, A. F., T. E. Feasby, L. Wilkie, and D. Lovgren. 1991. P2-peptide induced experimental allergic neuritis: a model to study axonal degeneration. *Acta Neuropathol. (Berl).* 82: 60–65.
15. Rostami, A., M. J. Brown, R. P. Lisak. A. J. Sumner, B. Zweiman, and D. E. Pleasure. 1984. The role of myelin P2 protein in the production of experimental allergic neuritis. *Ann. Neurol.* 16: 680–685.
16. Shy, M. E., E. Arroyo, J. Sladky, D. Menichella, H. Jiang, W. Xu, J. Kamholz, and S. S. Scherer. 1997. Heterozygous P0 knockout mice develop a peripheral neuropathy that resembles chronic inflammatory demyelinating polyneuropathy (CIDP). *J. Neuropathol. Exp. Neurol.* 56: 811–821.
17. Carenini, S., M. Maurer, A. Werner, H. Blazyca, K. V. Toyka, C. D. Schmid, G. Raivich, and R. Martini. 2001. The role of macrophages in demyelinating peripheral nervous system of mice heterozygously deficient in P0. *J. Cell Biol.* 152: 301–308.
18. Miyamoto, K., S. Miyake, M. Schachner, and T. Yamamura. 2003. Heterozygous null mutation of myelin P0 protein enhances susceptibility to autoimmune neuritis targeting P0 peptide. *Eur. J. Immunol.* 33: 656–665.
19. Khalili-Shirazi, A., P. Atkinson, N. Gregson, and R. A. Hughes. 1993. Antibody responses to P0 and P2 myelin proteins in Guillain-Barré syndrome and chronic idiopathic demyelinating polyradiculoneuropathy. *J. Neuroimmunol.* 46: 245–251.
20. Ilyas, A. A., F. A. Mithen, M. C. Dalakas, Z. W. Chen, and S. D. Cook. 1992. Antibodies to acidic glycolipids in Guillain-Barré syndrome and chronic inflammatory demyelinating polyneuropathy. *J. Neurol. Sci.* 107: 111–121.
21. Yan, W. X., J. J. Archelos, H. P. Hartung, and J. D. Pollard. 2001. P0 protein is a target antigen in chronic inflammatory demyelinating polyradiculoneuropathy. *Ann. Neurol.* 50: 286–292.

22. Kim, D. H., S. Muthyala, B. Soliven, K. Wiegmann, R. Wollmann, and E. Chelmicka-Schorr. 1994. The β_2-adrenergic agonist terbutaline suppresses experimental allergic neuritis in Lewis rats. *J. Neuroimmunol.* 51: 177–183.
23. Hasse, B., F. Bosse, and H. W. Muller. 2002. Proteins of peripheral myelin are associated with glycosphingolipid/cholesterol-enriched membranes. *J. Neurosci. Res.* 69: 227–232.
24. Caroni, P., and M. E. Schwab. 1988. Two membrane protein fractions from rat central myelin with inhibitory properties for neurite growth and fibroblast spreading. *J. Cell Biol.* 106: 1281–1288.
25. Iwase, T., C. G. Jung, H. Bae, M. Zhang, and B. Soliven. 2005. Glial cell line-derived neurotrophic factor-induced signaling in Schwann cells. *J. Neurochem.* 94: 1488–1499.
26. Winer, S., H. Tsui, A. Lau, A. Song, X. Li, R. K. Cheung, A. Sampson, F. Afifiyan, A. Elford, G. Jackowski, et al. 2003. Autoimmune islet destruction in spontaneous type 1 diabetes is not beta-cell exclusive. *Nat. Med.* 9: 198–205.
27. Martin, R. M., J. L. Brady, and A. M. Lew. 1998. The need for IgG2c specific antiserum when isotyping antibodies from C57BL/6 and NOD mice. *J. Immunol. Methods* 212: 187–192.
28. Rabinovitch, A., W. L. Suarez-Pinzon, O. Sorensen, R. C. Bleackley, and R. F. Power. 1995. IFN-γ gene expression in pancreatic islet-infiltrating mononuclear cells correlates with autoimmune diabetes in nonobese diabetic mice. *J. Immunol.* 154: 4874–4882.
29. Kolb, H. 1997. Benign versus destructive insulitis. *Diabetes Metab. Rev.* 13: 139–146.
30. Trembleau, S., G. Penna, S. Gregori, N. Giarratana, and L. Adorini. 2003. IL-12 administration accelerates autoimmune diabetes in both wild-type and IFN-γ-deficient nonobese diabetic mice, revealing pathogenic and protective effects of IL-12-induced IFN-γ. *J. Immunol.* 170: 5491–5501.
31. Jain, R., D. M. Tartar, R. K. Gregg, R. D. Divekar, J. J. Bell, H. H. Lee, P. Yu, J. S. Ellis, C. M. Hoeman, C. L. Franklin, and H. Zaghouani. 2008. Innocuous IFNγ induced by adjuvant-free antigen restores normoglycemia in NOD mice through inhibition of IL-17 production. *J. Exp. Med.* 205: 207–218.
32. Srinivasan, S., D. T. Bolick, D. Lukashev, C. Lappas, M. Sitkovsky, K. R. Lynch, and C. C. Hedrick. 2008. Sphingosine-1-phosphate reduces $CD4^+$ T-cell activation in type 1 diabetes through regulation of hypoxia-inducible factor short isoform I.1 and CD69. *Diabetes* 57: 484–493.
33. Bour-Jordan, H., H. L. Thompson, and J. A. Bluestone. 2005. Distinct effector mechanisms in the development of autoimmune neuropathy versus diabetes in nonobese diabetic mice. *J. Immunol.* 175: 5649–5655.
34. Zhu, Y., H. G. Ljunggren, E. Mix, H. L. Li, P. van der Meide, A. M. Elhassan, B. Winblad, and J. Zhu. 2001. Suppression of autoimmune neuritis in IFN-γ receptor-deficient mice. *Exp. Neurol.* 169: 472–478.
35. Park, H., Z. Li, X. O. Yang, S. H. Chang, R. Nurieva, Y. H. Wang, Y. Wang, L. Hood, Z. Zhu, Q. Tian, and C. Dong. 2005. A distinct lineage of CD4 T cells regulates tissue inflammation by producing interleukin 17. *Nat. Immunol.* 6: 1133–1141.
36. Bailey, S. L., B. Schreiner, E. J. McMahon, and S. D. Miller. 2007. CNS myeloid DCs presenting endogenous myelin peptides 'preferentially' polarize $CD4^+$ T_H-17 cells in relapsing EAE. *Nat. Immunol.* 8: 172–180.
37. Kroenke, M. A., T. J. Carlson, A. V. Andjelkovic, and B. M. Segal. 2008. IL-12- and IL-23-modulated T cells induce distinct types of EAE based on histology, CNS chemokine profile, and response to cytokine inhibition. *J. Exp. Med.* 205: 1535–1541.
38. Stromnes, I. M., L. M. Cerretti, D. Liggitt, R. A. Harris, and J. M. Goverman. 2008. Differential regulation of central nervous system autoimmunity by T_H1 and T_H17 cells. *Nat. Med.* 14: 337–342.
39. Bai, X. F., J. Zhu, G. X. Zhang, G. Kaponides, B. Hojeberg, P. H. van der Meide, and H. Link. 1997. IL-10 suppresses experimental autoimmune neuritis and down-regulates TH1-type immune responses. *Clin. Immunol. Immunopathol.* 83: 117–126.
40. Jander, S., J. Pohl, C. Gillen, and G. Stoll. 1996. Differential expression of interleukin-10 mRNA in Wallerian degeneration and immune-mediated inflammation of the rat peripheral nervous system. *J. Neurosci. Res.* 43: 254–259.
41. Lu, M. O., R. S. Duan, H. C. Quezada, Z. G. Chen, E. Mix, T. Jin, X. Yang, H. G. Ljunggren, and J. Zhu. 2007. Aggravation of experimental autoimmune neuritis in TNF-α receptor 1 deficient mice. *J. Neuroimmunol.* 186: 19–26.
42. Taylor, J. M., and J. D. Pollard. 2007. Soluble TNFR1 inhibits the development of experimental autoimmune neuritis by modulating blood-nerve-barrier permeability and inflammation. *J. Neuroimmunol.* 183: 118–124.
43. Gu, L., S. Tseng, R. M. Horner, C. Tam, M. Loda, and B. J. Rollins. 2000. Control of TH2 polarization by the chemokine monocyte chemoattractant protein-1. *Nature* 404: 407–411.
44. Kieseier, B. C., K. Krivacic, S. Jung, H. Pischel, K. V. Toyka, R. M. Ransohoff, and H. P. Hartung. 2000. Sequential expression of chemokines in experimental autoimmune neuritis. *J. Neuroimmunol.* 110: 121–129.
45. Gold, R., J. J. Archelos, and H. P. Hartung. 1999. Mechanisms of immune regulation in the peripheral nervous system. *Brain Pathol.* 9: 343–360.
46. Mathey, E. K., J. D. Pollard, and P. J. Armati. 1999. TNF α, IFN γ and IL-2 mRNA expression in CIDP sural nerve biopsies. *J. Neurol. Sci.* 163: 47–52.
47. Chen, Z., A. E. Herman, M. Matos, D. Mathis, and C. Benoist. 2005. Where $CD4^+CD25^+$ T reg cells impinge on autoimmune diabetes. *J. Exp. Med.* 202: 1387–1397.
48. Karandikar, N. J., C. L. Vanderlugt, J. A. Bluestone, and S. D. Miller. 1998. Targeting the B7/CD28:CTLA-4 costimulatory system in CNS autoimmune disease. *J. Neuroimmunol.* 89: 10–18.
49. Carreno, B. M., and M. Collins. 2002. The B7 family of ligands and its receptors: new pathways for costimulation and inhibition of immune responses. *Annu. Rev. Immunol.* 20: 29–53.
50. Zhu, Y., H. Ljunggren, E. Mix, H. L. Li, P. van der Meide, A. M. Elhassan, B. Winblad, and J. Zhu. 2001. CD28-B7 costimulation: a critical role for initiation and development of experimental autoimmune neuritis in C57BL/6 mice. *J. Neuroimmunol.* 114: 114–121.
51. Zhu, J., L. Zou, S. Zhu, E. Mix, F. Shi, H. Wang, I. Volkmann, B. Winblad, M. Schalling, and H. Ljunggren. 2001. Cytotoxic T lymphocyte-associated antigen 4 (CTLA-4) blockade enhances incidence and severity of experimental autoimmune neuritis in resistant mice. *J. Neuroimmunol.* 115: 111–117.
52. Chang, T. T., C. Jabs, R. A. Sobel, V. K. Kuchroo, and A. H. Sharpe. 1999. Studies in B7-deficient mice reveal a critical role for B7 costimulation in both induction and effector phases of experimental autoimmune encephalomyelitis. *J. Exp. Med.* 190: 733–740.
53. Girvin, A. M., M. C. Dal Canto, L. Rhee, B. Salomon, A. Sharpe, J. A. Bluestone, and S. D. Miller. 2000. A critical role for B7/CD28 costimulation in experimental autoimmune encephalomyelitis: a comparative study using costimulatory molecule-deficient mice and monoclonal antibody blockade. *J. Immunol.* 164: 136–143.
54. Kiefer, R., F. Dangond, M. Mueller, K. V. Toyka, D. A. Hafler, and H. P. Hartung. 2000. Enhanced B7 costimulatory molecule expression in inflammatory human sural nerve biopsies. *J. Neurol. Neurosurg. Psych.* 69: 362–368.
55. Hu, W., A. Janke, S. Ortler, H. P. Hartung, C. Leder, B. C. Kieseier, and H. Wiendl. 2007. Expression of CD28-related costimulatory molecule and its ligand in inflammatory neuropathies. *Neurology* 68: 277–282.
56. Murata, K., and M. C. Dalakas. 2000. Expression of the co-stimulatory molecule BB-1, the ligands CTLA-4 and CD28 and their mRNAs in chronic inflammatory demyelinating polyneuropathy. *Brain* 123(Pt. 8): 1660–1666.
57. Winer, S., I. Astsaturov, R. Cheung, L. Gunaratnam, V. Kubiak, M. A. Cortez, M. Moscarello, P. W. O'Connor, C. McKerlie, D. J. Becker, and H. M. Dosch. 2001. Type I diabetes and multiple sclerosis patients target islet plus central nervous system autoantigens; nonimmunized nonobese diabetic mice can develop autoimmune encephalitis. *J. Immunol.* 166: 2831–2841.
58. Miletic, H., O. Utermohlen, C. Wedekind, M. Hermann, W. Stenzel, H. Lassmann, D. Schluter, and M. Deckert. 2005. $P0_{106-125}$ is a neuritogenic epitope of the peripheral myelin protein P0 and induces autoimmune neuritis in C57BL/6 mice. *J. Neuropathol. Exp. Neurol.* 64: 66–73.
59. Zou, L. P., H. G. Ljunggren, M. Levi, I. Nennesmo, B. Wahren, E. Mix, B. Winblad, M. Schalling, and J. Zhu. 2000. P0 protein peptide 180–199 together with pertussis toxin induces experimental autoimmune neuritis in resistant C57BL/6 mice. *J. Neurosci. Res.* 62: 717–721.
60. Visan, L., I. A. Visan, A. Weishaupt, H. H. Hofstetter, K. V. Toyka, T. Hunig, and R. Gold. 2004. Tolerance induction by intrathymic expression of P0. *J. Immunol.* 172: 1364–1370.
61. Georgiou, J., and M. P. Charlton. 1999. Non-myelin-forming perisynaptic schwann cells express protein zero and myelin-associated glycoprotein. *Glia* 27: 101–109.
62. Levine, S., E. M. Hoenig, and M. W. Kies. 1968. Allergic encephalomyelitis: passive transfer prevented by encephalitogen. *Science* 161: 1155–1157.
63. Critchfield, J. M., M. K. Racke, J. C. Zuniga-Pflucker, B. Cannella, C. S. Raine, J. Goverman, and M. J. Lenardo. 1994. T cell deletion in high antigen dose therapy of autoimmune encephalomyelitis. *Science* 263: 1139–1143.
64. Hilliard, B. A., M. Kamoun, E. Ventura, and A. Rostami. 2000. Mechanisms of suppression of experimental autoimmune encephalomyelitis by intravenous administration of myelin basic protein: role of regulatory spleen cells. *Exp. Mol. Pathol.* 68: 29–37.
65. Odoardi, F., N. Kawakami, Z. Li, C. Cordiglieri, K. Streyl, M. Nosov, W. E. Klinkert, J. W. Ellwart, J. Bauer, H. Lassmann, et al. 2007. Instant effect of soluble antigen on effector T cells in peripheral immune organs during immunotherapy of autoimmune encephalomyelitis. *Proc. Natl. Acad. Sci. USA* 104: 920–925.
66. Su, M. A., D. Davini, Jr., K. Giang, M. S. Anderson, and H. Bour-Jordan. 2008. Specificity of autoantibody responses against neural proteins in a mouse model of autoimmune peripheral neuropathy. *J. Peripheral Nervous System* 13: 183.
67. Haq, R. U., W. W. Pendlebury, T. J. Fries, and R. Tandan. 2003. Chronic inflammatory demyelinating polyradiculoneuropathy in diabetic patients. *Muscle Nerve* 27: 465–470.
68. Sharma, K. R., J. Cross, O. Farronay, D. R. Ayyar, R. T. Shebert, and W. G. Bradley. 2002. Demyelinating neuropathy in diabetes mellitus. *Arch. Neurol.* 59: 758–765.
69. Krendel, D. A., D. A. Costigan, and L. C. Hopkins. 1995. Successful treatment of neuropathies in patients with diabetes mellitus. *Arch. Neurol.* 52: 1053–1061.
70. Gorson, K. C., A. H. Ropper, L. S. Adelman, and D. H. Weinberg. 2000. Influence of diabetes mellitus on chronic inflammatory demyelinating polyneuropathy. *Muscle Nerve* 23: 37–43.
71. Razavi, R., Y. Chan, F. N. Afifiyan, X. J. Liu, X. Wan, J. Yantha, H. Tsui, L. Tang, S. Tsai, P. Santamaria, et al. 2006. $TRPV1^+$ sensory neurons control beta cell stress and islet inflammation in autoimmune diabetes. *Cell* 127: 1123–1135.
72. Dalakas, M. C., M. Fujii, M. Li, and B. McElroy. 2000. The clinical spectrum of anti-GAD antibody-positive patients with stiff-person syndrome. *Neurology* 55: 1531–1535.

EJN fens EUROPEAN JOURNAL OF NEUROSCIENCE

European Journal of Neuroscience, Vol. 28, pp. 1049–1059, 2008 doi:10.1111/j.1460-9568.2008.06420.x

MOLECULAR AND DEVELOPMENTAL NEUROSCIENCE

Enhanced neurogenesis from neural progenitor cells with G1/S-phase cell cycle arrest is mediated by transforming growth factor β1

Sachiyo Misumi, Tae-Sun Kim, Cha-Gyun Jung, Tadashi Masuda, Susumu Urakawa, Yoshiaki Isobe, Fujiya Furuyama, Hitoo Nishino and Hideki Hida

Department of Neurophysiology and Brain Science, Nagoya City University Graduate School of Medical Sciences, 1 Kawasumi, Mizuho-cho, Mizuho-ku, Nagoya 467-8601, Japan

Keywords: aphidicolin, cdk5, NeuroD, rat neural progenitor cell, smad3

Abstract

We have previously demonstrated that a G1/S-phase cell cycle blocker, deferoxamine (DFO), increased the number of new neurons from rat neurosphere cultures, which correlated with prolonged expression of cyclin-dependent kinase (cdk) inhibitor $p27^{kip1}$ [H. J. Kim *et al.* (2006) *Brain Research*, 1092, 1–15]. The present study focuses on neuronal differentiation mechanisms following treatment of neural stem/progenitor cells (NPCs) with a G1/S-phase cell cycle blocker. The addition of DFO (0.5 mM) or aphidicolin (Aph) (1.5 μM) to neurospheres for 8 h, followed by 3 days of differentiation, resulted in an increased number of neurons and neurite outgrowth. DFO induced enhanced expression of transforming growth factor (TGF)-β1 and cdk5 at 24 h after differentiation, whereas Aph only increased TGF-β1 expression. DFO-induced neurogenesis and neurite outgrowth were attenuated by administration of a cdk5 inhibitor, roscovitine, suggesting that the neurogenic mechanisms differ between DFO and Aph. TGF-β1 (10 ng/mL) did not increase neurite outgrowth but rather the number of β-tubulin III-positive cells, which was accompanied by enhanced $p27^{kip1}$ mRNA expression. In addition, TGF-β receptor type II expression was observed in nestin-positive NPCs. Results indicated that DFO-induced TGF-β1 signaling activated smad3 translocation from the cytoplasm to the nucleus. In contrast, TGF-β1 signaling inhibition, via a TGF-β receptor type I inhibitor (SB-505124), resulted in decreased DFO-induced neurogenesis, in conjunction with decreased $p27^{kip1}$ protein expression and smad3 translocation to the nucleus. These results suggest that cell cycle arrest during G1/S-phase induces TGF-β1 expression. This, in turn, prompts enhanced neuronal differentiation via smad3 translocation to the nucleus and subsequent $p27^{kip1}$ activation in NPCs.

Introduction

Neural stem/progenitor cells (NPCs) possess self-renewing and multipotent capacities (Reynolds & Weiss, 1992; Gritti *et al.*, 1996), and are good donor cell candidates for cell transplantation in Parkinson's disease (Storch *et al.*, 2001). However, several problems still exist that should be addressed. Specifically, the regulation of neuronal differentiation, in particular dopaminergic differentiation, requires further study; most NPCs differentiate into glial cells and rarely into neurons (Yang *et al.*, 2002). To overcome this problem, it will be important to understand the mechanisms regulating neuronal differentiation in NPCs, as well as the differentiation of specific phenotypes.

Neuronal differentiation is tightly regulated by various factors (Ohnuma & Harris, 2003). Transcriptional factors (Math1, Mash1, etc.), cytokines (IFN-β, etc.) and trophic factors (PDGF, BDNF, NT-3, etc.) are involved in neuronal induction from NPCs (Williams *et al.*, 1997; Turnley *et al.*, 2002; Zhu *et al.*, 2002; Wong *et al.*, 2004; Bull & Bartlett, 2005; Lim *et al.*, 2007). In particular, transcriptional factors such as Nurr1, Lmx1a and Msx1 (Andersson *et al.*, 2007) as well as trophic factors such as sonic hedgehog, fibroblast growth factor-8 and transforming growth factor (TGF)-β (Roussa & Krieglstein, 2004) are reported to be determinants of midbrain dopaminergic neurons. We have previously reported that pleiotrophin, which is enhanced in the dopamine (DA)-depleted striatum and is highly expressed in neurospheres derived from mesencephalic tissue, promotes the survival and differentiation of DAergic, neurons (Hida *et al.*, 2003; Jung *et al.*, 2004). We recently reported that hypoxia-inducible factor 1α is involved in DAergic, differentiation from embryonic stem (ES)-derived NPCs (Kim *et al.*, 2008).

Central roles of cyclin-dependent kinase (cdk) inhibitors have been suggested in neural differentiation via a cell cycle arrest-independent mechanism (Ohnuma *et al.*, 2001; Joseph *et al.*, 2003; Vernon *et al.*, 2005). Two families of cdk inhibitors are known in mammals, the Ink4 and Cip/Kip families (Cunningham & Roussel, 2001). The members

Correspondence: Dr H. Hida, as above.
E-mail: hhida@med.nagoya-cu.ac.jp

Received 19 March 2008, revised 4 July 2008, accepted 22 July 2008

of the Cip/Kip family have been identified as $p21^{cip}$, $p27^{kip1}$ and $p57^{kip2}$ (Dyer & Cepko, 2001). $p57^{kip1}$ and $p27^{kip1}$ not only inhibit the cell cycle but also influence cell fate (Dyer & Cepko, 2001). In particular, $p27^{kip1}$ has been shown to play an essential role in neuronal differentiation (Ohnuma *et al.*, 1999; Levine *et al.*, 2000; Carruthers *et al.*, 2003), as well as lengthening of the G1-phase in NPCs (Mitsuhashi *et al.*, 2001). Although the relationship between cell cycle control and NPC differentiation is not completely understood, differentiation timing is determined by a defined number of cell divisions, which is dependent on the cell cycle inhibitor $p27^{kip1}$ (Casaccia-Bonnefil *et al.*, 1999).

We have previously shown that pre-treatment with deferoxamine (DFO), a G1/S-phase blocker, increased neuronal, not astrocytic, NPC differentiation (Kim *et al.*, 2006), which suggests that prolonged elevation of $p27^{kip1}$ expression is involved in neuronal differentiation after cell cycle arrest. To understand how neuronal differentiation is regulated in NPCs, using DFO as well as a popular G1/S-phase cell cycle blocker [aphidicolin (Aph)], we focused on the mechanism of DFO-induced $p27^{kip1}$ expression, which is related to enhanced neuronal differentiation by G1/S-phase inhibitors.

Materials and methods

Neurosphere cultures

Our experiment was approved by the committee of the Institute for Experimental Animal Science, Nagoya City University Medical School. Pregnant Wistar rats [embryonic day (E)12] were obtained from Japan SLC, Inc. (Hamamatsu, Shizuoka, Japan). Ventral mesencephalic tissues were obtained from E12.5 rat embryos of mother rats under deep anesthesia with pentobarbital (> 50 mg/kg, i.p.) and tissues were mechanically dissociated to create cell suspensions. The cells were plated on 75-cm^2 culture dishes (10 mL of 2×10^5 cells/mL) and cultured in expansion medium (Dulbecco's modified Eagle's medium, DMEM/F12 containing N_2 supplement) supplemented with 20 ng/mL fibroblast growth factor-2 (PeproTech, London, UK). The medium was changed every other day and fibroblast growth factor-2 (20 ng/mL) was added daily. At the end of the expansion (4 days *in vitro*), cells were resuspended and replated on culture dishes at a density of 2×10^5 cells/mL. At 1 day after first passage (P1D1), cells were treated with 0.5 mM DFO (Sigma, St Louis, MO, USA) or Aph (Sigma) for 8 h in expansion medium. After washing three times with phosphate-buffered saline (PBS), cells were plated into six wells of a 1.9-cm^2 culture dish (Nunc, Roskilde, Denmark) containing 13-mm diameter coverglass (Matsunami Glass Ind. Ltd, Osaka, Japan) pre-coated with poly-L-ornithine/fibronectin (15 μg/mL/1 μg/mL) and cultured in differentiation medium (DMEM/F12 containing N_2 supplement and 1% fetal calf serum) for 3 days.

Immunohistochemistry

Cells cultured on coverglasses were fixed in pre-cooled acetic ethanol (95%, −20°C) for 20 min, washed, permeated in 0.25% Triton-X100/PBS and blocked with 3% horse serum. Cells were then incubated with mouse anti-β-tubulin III monoclonal antibody (1 : 500; Sigma) or anti-microtubule-associated protein-2 (MAP-2) monoclonal antibody (1 : 500; Chemicon, Temecula, CA, USA) at 4°C overnight. After washing in 0.25% Triton-X100/PBS, cells were incubated with biotinylated anti-mouse serum, followed by development with a Vector ABC kit and 3′3-diaminobenzidine chromagen.

For each experiment, the number of β-tubulin III- and MAP-2-positive cells, as well as total cells (hematoxylin-positive cells), was counted in 10 randomly selected fields from a 13-mm diameter circular coverglass. One coverglass was used for each staining paradigm (β-tubulin III or MAP-2) with each treatment (DFO or Aph). More than three independent experiments were performed for each group and analysis was performed using a bright field microscope (AX70; Olympus, Tokyo, Japan) at 40× magnification. Depending on the culture condition, there was a slight variation in the total number of cells from the 10 randomly selected fields (mean ± SD: 4011 ± 436 cells in control, $n = 7$; 3296 ± 592 cells in DFO treatment, $n = 7$; 3809 ± 406 cells in Aph treatment, $n = 6$). For this reason, the percentage of total cells from each independent experiment is represented by mean + SEM. The total number of positive cells from the three independent experiments was also presented as mean ± SEM.

For the assessment of neurite extensions, β-tubulin III-positive cells were observed under an Olympus AX-70 microscope and digital images were taken using an Olympus DP-70 microscope-mounted digital camera. The length of the longest neurite in each β-tubulin III-positive cell was measured by NIH imaging and expressed as mean ± SEM. To effectively represent the distribution pattern, neurite outgrowth was categorized into five classifications (0–30, 30–60, 60–90, 90–120 and = 120 μm) and presented as a percentage of total cells.

Immunofluorescence detection

Cells were incubated with anti-TGF-β receptor (TGF-βR) type II (1 : 200; Upstate, Lake Placid, NY, USA), anti-nestin (1 : 100; Chemicon) and anti-smad3 (1 : 100; Santa Cruz, CA, USA) antibodies, followed by fixation in 4% paraformaldehyde for 20 min at 4°C. The positive-labeled cells were visualized with Alexa 488- and Alexa 594-conjugated anti-rabbit IgG antibodies (Molecular Probes, Eugene, OR, USA). Cell nuclei were also stained with 4′, 6-Diamidino-2-phenylindole (DAPI). Fluorescent images were obtained using an LSM5 confocal laser-scanning microscope (Carl Zeiss, Göttingen, Germany). The number of total cells and smad3-positive cells were counted from the DAPI nuclear staining and smad3 staining, respectively. Data are represented by the percentage of total cells from three independent experiments as mean ± SEM.

Treatment with TGF-β1 and blocking its effect with an inhibitor

The NPCs were allowed to differentiate for 3 days with differentiation medium supplemented with TGF-β1 (10 ng/mL or 200 pg/mL). Cell counts of β-tubulin III-positive cells, as well as neurite outgrowth and gene expression ($p27^{kip1}$ and cdk5), were investigated at 3 days after differentiation. Data from the total number of positive cells of three independent experiments were presented as mean ± SEM. The distribution pattern of neurite outgrowth was categorized by a five-grade classification (0–30, 30–60, 60–90, 90–120 and > 120 μm) as a percentage of total cells.

The TGF-β signaling was blocked by treatment with 1 μM SB-505124 (SB) (Sigma) prior to switching to differentiation medium. Western blot of $p27^{kip1}$ protein expression and cell counts of β-tubulin III- or smad3-positive cells were performed at 3 days after differentiation.

Real-time PCR

Total RNA was isolated using Trizol reagent (Invitrogen, Carlsbad, CA, USA) and polymerase chain reaction (PCR) was performed by incubation at 95°C for 10 min followed by 40 cycles of 15 s at 95°C, 1 min at 60°C, 45 s at 72°C and 15 s at 80°C (for SYBR Green detection) using an ABI Prism 7000 Sequence Detection System

(Applied Biosystems, Foster, CA, USA) as previously reported (Kim *et al.*, 2006). As glyceraldehyde-3-phosphate dehydrogenase and β-actin expression were confirmed to remain constant following DFO treatment, glyceraldehyde-3-phosphate dehydrogenase mRNA was used as an internal control. Therefore, the expression of each gene was normalized by a corresponding amount of glyceraldehyde-3-phosphate dehydrogenase mRNA. Amplification was performed with the following primers: glyceraldehyde-3-phosphate dehydrogenase, 5′-TGTGTCCGTCGTGGATCTGA-3′ and 5′-CCTGCTTCACCACCTTCTTGA-3′; β-actin, 5′-AGGCCAACCGTGAAAAGATG-3′ and 5′-GCCTGGATGGCTACGTACATG-3′; $p27^{kip1}$, 5′-GGCGAAGAGAACAGAAGAAAATG-3′ and 5′-GGGCGTCTGCTCCACAGT-3′; cdk5, 5′-TGTGGCTCTGAAGCGAGTCA-3′ and 5′-TCCCGGAGGGCTGAACTT-3′; p35, 5′-TGAAATCTCCTACCCGCTCAA-3′ and 5′-GAGGCAACGGTCCCAAAA-3′; p39, 5′-GGAAGTGCACCCCCAACTT-3′ and 5′-GGGCAGAAATGGAAAGATGGA-3′; TGF-β1, 5′-AAACGGAAGCGCATCGAA-3′ and 5′-GGGACTGGCGAGCCTTAGTT-3′; TGF-β2, 5′-AGGGTCTTTCGCTTGCAGAA-3′ and 5′-TTGGATTTAAGGATCTGATACAGTTCA-3′; TGF-β3, 5′-GCGTCTCAAGAAGCAGAAGGA-3′ and 5′-TCGGTGTGGAGGAATCATCA-3′.

Western blot analysis

Cell were washed with PBS and harvested in lysis buffer (50 mM HEPES, pH 7.8, 150 mM NaCl, 150 mM $MgCl_2$, 0.1 mM EDTA, 0.1% sodium dodecyl sulfate, 1% Triton X-100) containing a protease inhibitor cocktail (Sigma). Cells were homogenized and incubated on ice for 30 min. The protein was harvested by centrifugation at 12 000 ***g*** at 4°C and the protein concentration of the supernatant was assayed using the Bradford assay. Twenty micrograms of each sample were loaded onto a 10% polyacrylamide gel and transferred to a polyvinylidene difluoride membrane (Millipore, Billerica, MA, USA). For western blot analysis, the membrane was blocked (5% skim milk and 0.1% Tween-20 in PBS) and incubated with anti-mouse $p27^{kip1}$ (1 : 2500; BD Bioscience, San Jose, CA, USA) and anti-α-tubulin (1 : 8000; Sigma) antibodies. The secondary antibody was peroxidase-conjugated anti-mouse IgG (1 : 2000; Sigma). Immunoreactive signals were detected with ELC™ western blotting detection reagent (GE Healthcare, Buckinghamshire, UK).

ELISA detection

Cells were homogenized in ice-cold lysis/extraction reagent (Sigma) and incubated for 15 min on ice. The protein was harvested by centrifugation at 12 000 ***g*** at 4°C for 10 min. The Bradford assay was employed to determine the protein concentration. The amount of TGF-β1 was measured by Quantikine ELISA kit (R&D Systems, Minneapolis, MN, USA) following the manufacturer's recommended protocols.

Statistical analysis

Cell counts of β-tubulin III- or MAP-2-positive cells, as well as measurement of neurite outgrowth, were evaluated using one-factor ANOVA followed by post-hoc Fisher's PLSD test to correct for multiple analysis or Student's *t*-test for comparison between two groups with values of $P < 0.05$. To detect statistical significance in mRNA expression using real-time PCR, Mann–Whitney test was used for comparison with control. To evaluate the effect of roscovitine (Ros) or SB on DFO action, one-factor ANOVA followed by *post-hoc* Scheffe test was used with values of $P < 0.05$.

Results

Cell cycle arrest in G1/S-phase increased amount of neurogenesis and neurite outgrowth

The NPCs obtained from E12.5 rat ventral mesencephalon were cultured with expansion medium for 4 days, supplemented with 20 ng/mL fibroblast growth factor-2, followed by passage at P0D4. NPCs were treated with cell cycle blockers of G1/S-phase for 8 h on P1D1. Optimal concentrations of DFO (0.5 mM) and Aph (1.5 μM) were used for this study based on our previous report (Kim *et al.*, 2006) demonstrating that NPC proliferation was effectively arrested with no cell toxicity in this condition. After washing, cells were allowed to differentiate for 3 days followed by immunostaining for β-tubulin III and MAP-2 (Fig. 1A). Depending on the culture condition used, there was a slight variation in the total number of cells within selected fields using our method. Therefore, the number of β-tubulin III- and MAP-2-positive cells was represented as the percentage of total cells from three independent experiments, as well as the number of positive cells and total cells.

The DFO treatment increased the number of β-tubulin III-positive cells (555 ± 76 cells in 3141 ± 262 total cells; 17.5 ± 1.0% of total cells, $n = 3$, $P < 0.01$) compared with control (471 ± 31 cells in 3930 ± 110 total cells; 12.0 ± 0.8% of total cells, $n = 3$), whereas Aph addition increased that of the positive cells (533 ± 38 cells in 3511 ± 157 total cells; 15.2 ± 0.4% of total cells, $n = 3$, $P < 0.05$) (Fig. 1B and C). The number of MAP-2-positive cells was also increased by DFO (617 ± 26 cells in 3738 ± 219 total cells; 16.6 ± 0.4% of total cells, $n = 3$) compared with control (537 ± 25 cells in 4312 ± 238 total cells; 12.5 ± 0.8% of total cells, $n = 3$, $P < 0.01$), whereas Aph addition increased that of the positive cells (640 ± 25 cells in 4091 ± 146 total cells; 15.7 ± 0.5% of total cells, $n = 3$, $P < 0.05$) (Fig. 1D).

Assessment of the longest neurite in each β-tubulin III-positive cell revealed that neurite length was significantly longer in the DFO-treated (69.9 ± 1.7 μm, $n = 227$, $P < 0.01$) and Aph-treated (66.8 ± 1.9 μm, $n = 206$, $P < 0.01$) groups compared with the control group (56.3 ± 2.7 μm, $n = 209$) (Fig. 1E). There was no difference in the number of neurites from a positive cell between control, DFO-treated and Aph-treated groups (data not shown).

Cdk5 signaling in enhanced neuronal differentiation after cell cycle arrest

Cyclin-dependent kinase 5 is involved in neurite outgrowth (Nikolic *et al.*, 1996) and interacts with $p27^{kip1}$ protein to influence neuronal migration (Kawauchi *et al.*, 2006). To investigate whether cdk5 and its binding proteins, p35 and p39, are involved in neurite outgrowth following DFO treatment and Aph treatment, real-time PCR was utilized to measure cdk5, p35 and p39 expression (Fig. 2A). Expression of cdk5 was significantly elevated at 24 h after DFO treatment (2.67 ± 0.47-fold compared with control, $n = 4$, $P < 0.05$), whereas p35 expression was decreased (0.83 ± 0.08-fold, $n = 4$) and p39 expression remained unchanged (0.95 ± 0.12-fold, $n = 5$). Aph administration did not cause significant elevation of cdk5 (1.41 ± 0.18-fold, $n = 4$), p35 (0.95 ± 0.12, $n = 4$) or p39 (0.91 ± 0.23, $n = 4$) expression.

To inhibit the effect of cdk5, a cdk5 kinase inhibitor (Ros) was added to cells during differentiation. As treatment with 5-10 μM Ros induced cell toxicity in NPCs, 3 μM Ros was used for this experiment and no toxic effects were exhibited. Ros decreased the number of β-tubulin III-positive cells (DFO: 16.7 ± 1.7% of total cells, $n = 5$; DFO + Ros: 8.71 ± 1.7%, $n = 4$, $P < 0.01$) to the control level (10.7 ± 1.0%, $n = 5$) (Fig. 2B). In addition, Ros treatment resulted in decreased neurite length (DFO ± Ros: 42.7 ± 1.9 μm, $n = 183$, $P < 0.01$).

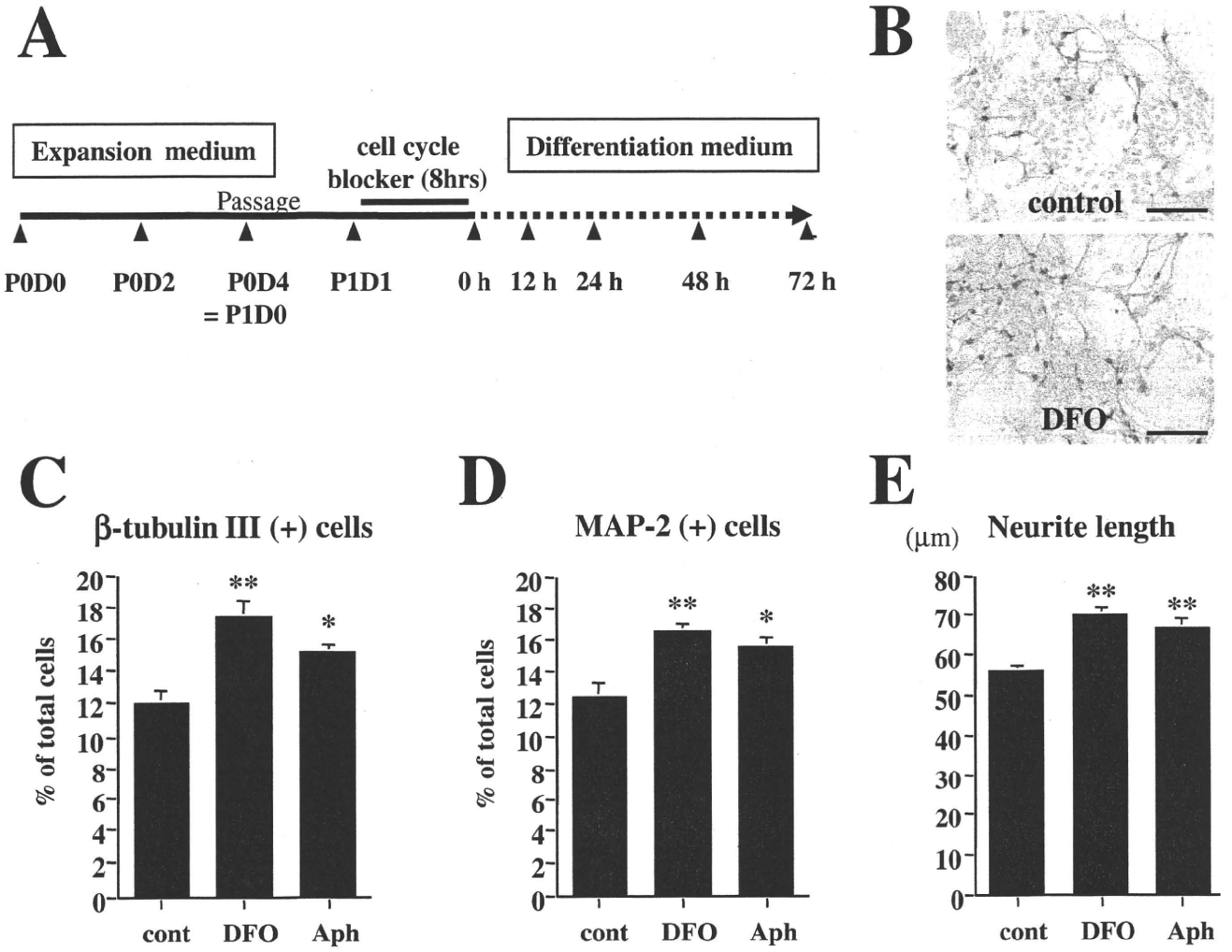

FIG. 1. G1/S-phase cell cycle inhibition of neurospheres increases the number and neurite length of neurons after differentiation. (A) Schema of experimental protocol. Neurospheres were expanded in expansion medium containing 20 ng/mL fibroblast growth factor (FGF)-2 and the medium was changed every other day. FGF-2 was added daily to the medium. After 4 days with no passage (P0D4), neurospheres were resuspended and replated at a density of 2×10^5 cells/mL [at the day of the first passage (P1D0)], allowing for secondary neurospheres. At 1 day after the first passage (P1D1), cell cycle inhibitors of G1/S-phase (DFO or Aph) were added to expansion medium for 8 h, followed by differentiation for 3 days in differentiation medium on poly-L-ornithine- and fibronectin-coated coverglasses. (B) Treatment with DFO (lower panel) increased the number of β-tubulin III-positive cells and neurite length compared with non-treated control cultures (upper panel). Scale bar, 100 μm. For each experiment, the numbers of β-tubulin III-positive (C) and MAP-2-positive (D) cells, as well as total cells, were counted in 10 randomly selected fields from a 13-mm diameter circular coverglass. A total of three independent experiments were performed, with one coverglass per staining paradigm (β-tubulin III or MAP-2) for each treatment (DFO or Aph). Data are represented by the percentage of total cells from three independent experiments as mean ± SEM. DFO ($n = 3$) and Aph ($n = 3$) treatment increased the number of β-tubulin III-positive (C) and MAP-2-positive (D) cells. Note that more β-tubulin III-positive and MAP-2-positive cells were detected in the DFO-treated and Aph-treated groups compared with control (cont), whereas fewer total cells were observed in the DFO-treated and Aph-treated groups compared with control ($n = 3$). (E) The length of the longest neurite in each β-tubulin III-positive cell was measured by NIH imaging. The neurite length induced by DFO or Aph was significantly longer than those in non-treated control. Note that no significant difference in neurite number was shown between groups. $^*P < 0.05$ and $^{**}P < 0.01$ as compared with control (cont).

Distribution patterns of neurite length in control, DFO-treated and DFO + Ros-treated groups are shown in Fig. 2D. Although the percentage of β-tubulin III-positive cells with longer neurites (> 90-μm) was increased by DFO treatment compared with control, Ros administration attenuated DFO-induced neurite outgrowth, resulting in almost 50% of cells with shorter neurites (< 60 μm) (Fig. 2D).

Expression of TGF-β1 was induced by G1/S-phase cell cycle inhibitors

Transforming growth factor-β regulates cell differentiation and controls the cdk inhibitor-mediated cell cycle, such as $p21^{cip1}$ expression in the central nervous system (Farkas *et al.*, 2003; Siegenthaler & Miller, 2005), indicating that TGF-β is a candidate factor that links cell cycle control and differentiation. To clarify whether TGF-β was involved in enhanced neuronal differentiation following DFO treatment, expression of TGF-β isoforms (β1-3) was investigated in DFO-treated NPCs using real-time PCR (Fig. 3A).

Although expression of TGF-β1 mRNA decreased at the endpoint of DFO treatment (0.62-fold less than control), it was significantly elevated in the DFO-treated group at 24 h after differentiation (5.35 ± 1.07-fold of control, $n = 4$, $P < 0.05$). TGF-β1 expression returned to control levels (0.93 ± 0.17-fold of control, $n = 4$)

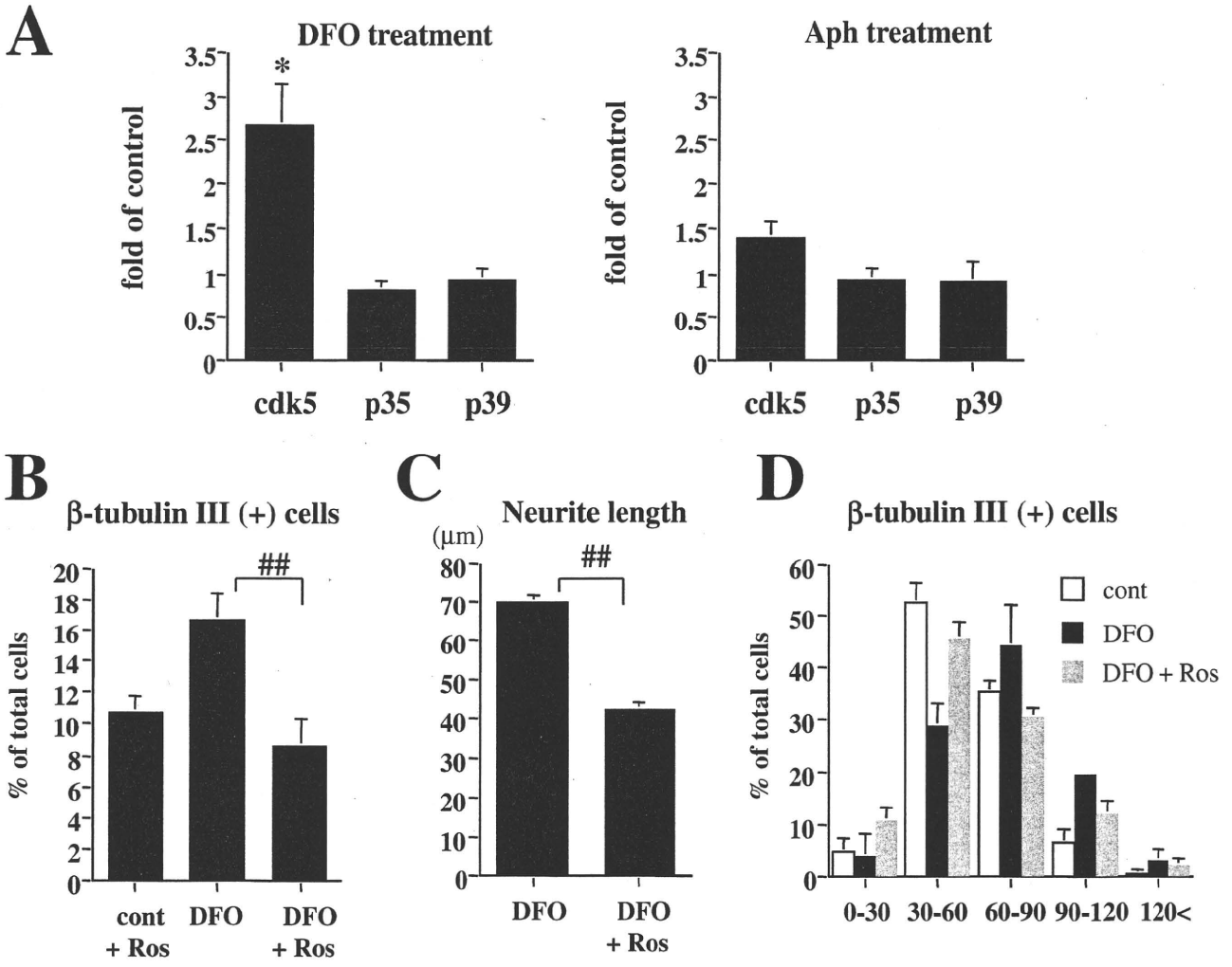

FIG. 2. The DFO-induced increase in the number of neurons and neurite outgrowth is mediated by cdk5. (A) Expression of cdk5, p35 and p39 mRNA was measured at 24 h after differentiation using real-time PCR. DFO treatment increased cdk5 expression, although expression of p35 and p39 did not change. Aph treatment did not result in a significant enhancement of either gene, indicating that the mechanism is, at least in part, different from DFO. (B–D) Ros, a cdk5 kinase inhibitor, resulted in significantly inhibited DFO-induced neurite outgrowth. A non-toxic level of Ros (3 μM) was given to cells during differentiation, followed by β-tubulin III immunostaining. The numbers of β-tubulin III-positive cells were counted in 10 randomly selected fields for each experiment, with a total of four to five independent experiments (B). Ros significantly decreased the number of β-tubulin III-positive cells to the control (cont) level ($P < 0.01$). The length of the longest neurite in each β-tubulin III-positive cell was measured in Ros-treated cells (C). Ros addition caused a significant decrease of DFO-induced neurite length (DFO + Ros: 42.7 ± 1.9 μm, $n = 183$, $P < 0.01$). (D) Distribution patterns of neurite length in control, DFO-treated and DFO + Ros-treated groups. Distribution of neurite length was altered by Ros treatment, showing that the percentage of β-tubulin III-positive cells with neurites that are 60–90 or > 60 μm long was decreased, whereas an increase in cells with shorter neurites was observed in the Ros-treated group ($n = 3$). $^{*}P < 0.05$ as compared to control $^{\#\#}P < 0.01$ for comparison between DFO and DFO + Ros.

by 72 h after treatment. Expression of the TGF-β2 and -β3 isoforms was not different between the DFO-treated and control groups but, during differentiation, expression gradually increased. At 24 h after differentiation, assessment of protein levels by ELISA assay also revealed that TGF-β1 increased after DFO treatment in neurosphere cultures (control: 128.6 pg/mL; DFO: 214.3 pg/mL, $n = 2$).

To investigate whether enhanced expression of TGF-β1 was induced in G1/S-phase cell cycle blockers in general, a popular blocker, Aph (1.5 μM), was also administered to NPCs. TGF-β1 and $p27^{kip1}$ expression was subsequently measured 24 h later (Fig. 3B). Aph induced enhanced expression of TGF-β1 mRNA (6.62 ± 0.68-fold of control, $n = 3$, $P < 0.05$) and $p27^{kip1}$ mRNA (1.98 ± 0.30-fold, $n = 4$, $P < 0.05$), indicating that enhanced expression of TGF-β1and $p27^{kip1}$ during differentiation could be a general response of NPCs to the treatment of G1/S-phase cell cycle blockers.

Effects of TGF-β1 on NPCs were different from those of DFO

To examine the effect of TGF-β1 on neuronal differentiation, neurospheres were treated with 10 ng/mL TGF-β1 followed by quantification of β-tubulin III-positive cells and total cells (Fig. 4A). TGF-β1 increased the number of β-tubulin III-positive cells (640.7 ± 32.7 cells in 5252 ± 273.6 total cells; 12.20 ± 0.09% of total cells, $n = 3$, $P < 0.01$) compared with control cultures (477.3 ± 8.2 cells in 4948 ± 218.3 total cells; 9.66 ± 0.32% of total cells, $n = 3$). There was no difference, however, in the length of the longest neurite following TGF-β1 treatment (57.94 ± 1.60 μm, $n = 139$) compared with the control group (61.38 ± 1.52 μm, $n = 148$) (Fig. 4B), showing similar distribution patterns in neurite outgrowth (Fig. 4C).

Real-time PCR was utilized to measure expression of $p27^{kip1}$ and cdk5 (Fig. 4D). TGF-β1 enhanced $p27^{kip1}$ mRNA expression at 24 h

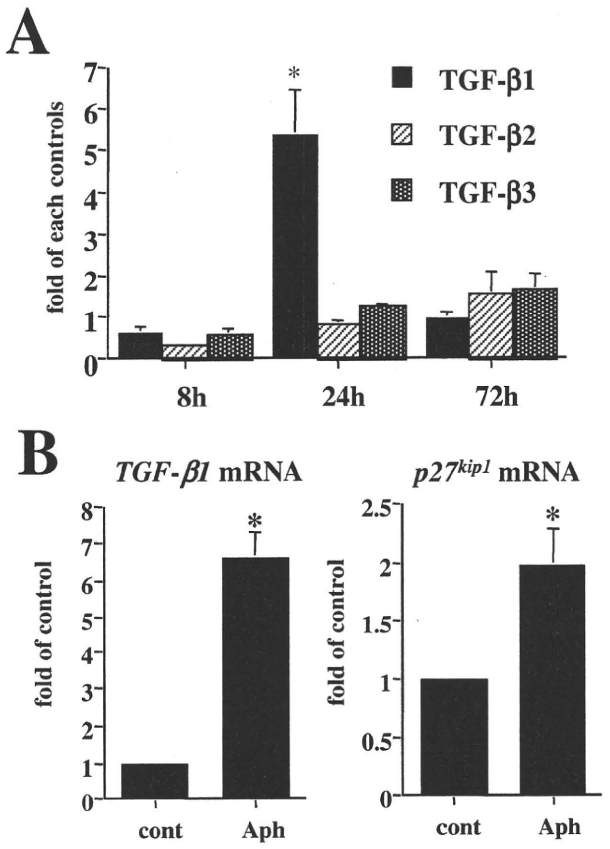

FIG. 3. Enhanced TGF-β1 expression observed during differentiation following G1/S-phase cell cycle inhibition. (A) Expression of TGF-β1, -β2 and -β3 was measured by real-time PCR at 0, 24 and 72 h after DFO treatment. Expression of TGF-β1 mRNA significantly increased with DFO treatment after 24 h of differentiation (5.35 ± 1.07, $n = 4$) but was not changed after 0 and 72 h. Note that expression of TGF-β2 and -β3 was not altered by DFO treatment until 72 h ($n = 3$). (B) A popular G1/S-phase cell cycle blocker, Aph (1.5 μM), was administered to NPCs and TGF-β1 expression was subsequently measured. At 24 h after addition of Aph, expression of TGF-β1 mRNA increased, showing that enhanced expression of TGF-β1 was induced in G1/S-phase cell cycle blockers in general. Enhanced expression of $p27^{kip1}$ mRNA was, similar to the elevation by DFO administration, detected at 24 h after Aph treatment. cont, control. *$P < 0.05$ as compared to control.

after treatment compared with control (1.91 ± 0.28-fold of control, $n = 6$, $P < 0.05$). However, TGF-β1 did not increase expression of cdk5 mRNA (1.08 ± 0.09-fold, $n = 3$), revealing differential responses in cdk5 expression between TGF-β1 and DFO or Aph.

DFO inhibition of TGF-β1 signal resulted in decreased $p27^{kip1}$ expression and β-tubulin III-positive cells

To confirm that TGF-β1 was involved in enhanced $p27^{kip1}$ expression following DFO treatment, cells were treated with a TGF-βR type I blocker (SB, 1 μM) followed by $p27^{kip1}$ protein quantification (Fig. 5). SB treatment alone did not alter $p27^{kip1}$ protein levels compared with control (Fig. 5A, lanes 1 and 2). Administration of DFO or TGF-β1 to NPCs resulted in significantly increased $p27^{kip1}$ protein expression at 24 h after treatment (Fig 5A, lanes 3 and 5); however, administration of SB significantly blocked the DFO- or TGF-β1-enhanced $p27^{kip1}$ protein expression (Fig. 5A, lanes 4 and 6, $n = 3$-4, $P < 0.01$ for DFO vs. DFO + SB and $P < 0.05$ for TGF-β1 vs. TGF-β1 + SB).

Expression of TGF-βR type II on NPCs was confirmed by immunofluorescence staining (Fig 5B). Many TGF-βR type II-positive cells (Fig 5B, upper left panel), as well as nestin-positive cells (Fig. 5B, upper right panel), were observed. Most TGF-βR type II-positive cells were also nestin-positive (Fig. 5B, lower panel, arrow), whereas some cells were nestin-negative (Fig. 5B, lower panel, arrowhead).

Treatment with SB was effective in significantly reducing the DFO-induced increase of β-tubulin III-positive cells to control level (12.46 ± 0.51% of total cells, $n = 3$, $P < 0.01$), whereas SB did not show a significant effect on non-treated controls (Fig. 5C).

DFO treatment induces smad3 translocation to the nucleus

Transforming growth factor-β acts in cells through smads, which accumulate in the nucleus and form complexes that control target genes (ten Dijke & Hill, 2004; Massague *et al.*, 2005). To investigate whether DFO treatment activates smad signaling, smad3 localization in NPCs was analysed by immunofluorescence staining. Results revealed that smad3 was primarily expressed in the cytoplasm of control groups at 24 h after differentiation (Fig. 6A, upper panels). In addition, smad3 localization was observed in the majority of TGF-β1 (10 ng/mL)-treated cells (Fig. 6A, lower panels). DFO induced smad3 translocation to the nucleus (Fig. 6A, middle panels).

In the DFO-treated group, the percentage of cells with nuclear smad3 staining (19.58 ± 1.97% of the total cells, $n = 5$, $P < 0.01$) was greater than the control group (8.26 ± 0.69%, $n = 5$) (Fig. 6B). However, when SB was added to the DFO-treated NPCs, there was a significant decrease in the number of nuclear smad3-positive cells (10.08 ± 0.25% of total cells, $n = 3$, $P < 0.01$). In contrast, addition of TGF-β1 (200 pg/mL) resulted in an increase of smad3-positive cells (21.02 ± 1.33%, $n = 3$, $P < 0.01$), which was similar to the level in the DFO treatment group.

Discussion

The present study aimed to elucidate the relationship between cell cycle regulation and neuronal differentiation, with a focus on mechanisms of neuronal differentiation after DFO-mediated cell cycle regulation. Results demonstrated that: (i) G1/S-phase cell cycle blockers, such as DFO and Aph, enhanced neurogenesis and neurite extension; (ii) G1/S-phase cell cycle arrest increased TGF-β1 expression during differentiation; (iii) in NPC cultures, TGF-β1 increased β-tubulin III-positive cells, in conjunction with $p27^{kip1}$ expression; (iv) NPCs expressed TGF-βR type II; (v) inhibition of TGF-β1 signaling blocked DFO-induced $p27^{kip1}$ elevation and DFO-induced neurogenesis, and (vi) DFO, using a concentration that was comparable to 200 pg/mL TGF-β1, induced smad3 translocation from the cytoplasm to the cell nucleus.

We have previously reported that DFO increased the number of neurons in neurosphere cultures and our results showed that this was due to prolonged $p27^{kip1}$ expression (Kim *et al.*, 2006). The signaling pathway for $p27^{kip1}$ expression after DFO treatment was analysed in the present study, which provided a hypothesis for mechanisms of neuronal differentiation by G1/S-phase cell cycle inhibitors (Fig. 7).

TGF-β1 expression was induced by G1/S-phase cell cycle blockers

The present results demonstrated increased TGF-β1 expression in DFO- or Aph-treated neurosphere cultures that had undergone

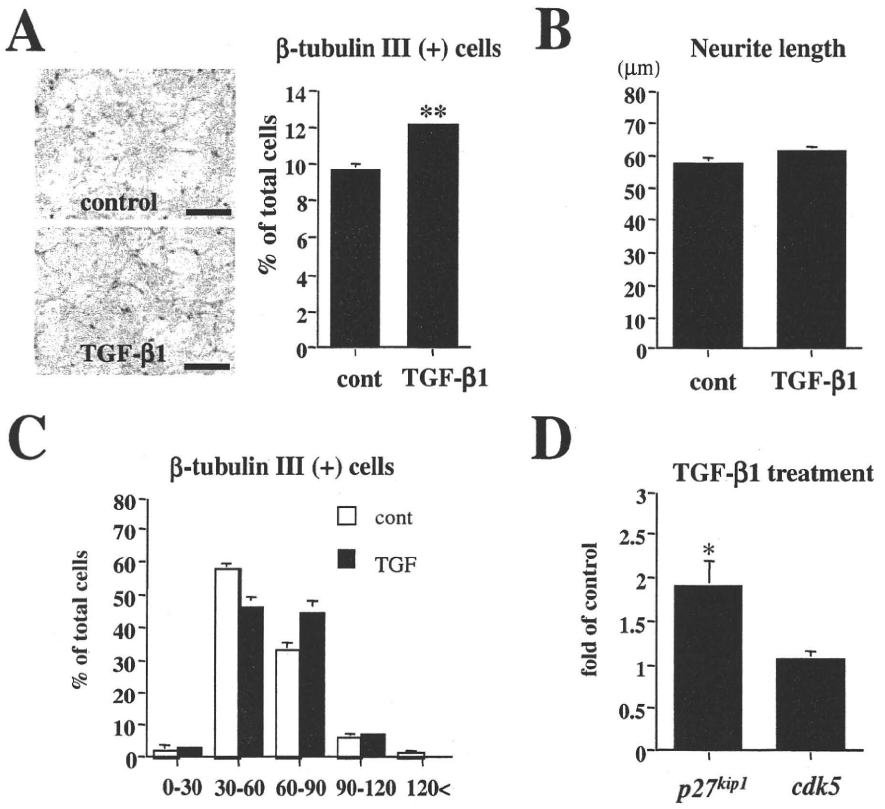

FIG. 4. TGF-β1 treatment of neurospheres increased the number of neurons rather than neurite outgrowth. Neurospheres were treated with TGF-β1 (10 ng/mL), followed by quantification of β-tubulin III-positive cells (A), measurement of neurite length (B), distribution pattern of neurite (C) and mRNA expression of $p27^{kip1}$ and cdk5 (D). (A) TGF-β1 caused an increase in the number of β-tubulin III-positive neurons ($P < 0.01$) compared with control (cont) cultures. Scale bar, 100 μm. (B) There was no difference in the length of the longest neurite after TGF-β1 treatment. (C) Distribution pattern of the longest neurite length after TGF-β1 treatment was similar to non-treated controls. (D) Expression of $p27^{kip1}$ mRNA was enhanced by TGF-β1 at 24 h after treatment ($n = 6$). Expression of cdk5 mRNA in TGF-β1 treatment was similar to the control level ($n = 6$), revealing a different response of TGF-β1 in cdk5 expression compared with DFO. $*P < 0.05$ and $**P < 0.01$ as compared with control.

neuronal differentiation. It has been reported that TGF-β1 acts as an anti-proliferative factor and arrests cell cycle during G1-phase, due to reduced cyclin expression and increased cdk inhibitor ($p21^{cip1}$, $p27^{kip1}$) expression (Polyak *et al.*, 1994; Bouchard *et al.*, 1997; Ko *et al.*, 1998; Yoo *et al.*, 1999; Wolfraim *et al.*, 2004). However, it has also been shown that DFO induced senescence-like G1 arrest associated with induction of $p27^{kip1}$ through TGF-β1 (Yoon *et al.*, 2002). Therefore, it is likely that a positive feedback loop is involved when treating NPCs with G1/S-phase cell cycle blockers. A G1/S-phase cell cycle blocker, such as DFO or Aph, increased TGF-β1-induced G1 arrest followed by $p27^{kip1}$ activation, and then activated $p27^{kip1}$ further induced cell cycle arrest in G1-phase. Although mechanisms of TGF-β1 expression in NPCs are poorly understood, it seems likely that TGF-β1 expression increases during G1/S-phase cell cycle arrest, which was supported by increased TGF-β1 expression after Aph (a popular G1/S-phase cell cycle blocker) treatment.

TGF-βR type I signaling induced nuclear translocation of smad3

Smads, which are key molecules involved in TGF-β1 signaling, are known to target neurogenic genes within the nucleus (Sun *et al.*, 2001). The present study demonstrated translocation of smad3 to the nucleus after DFO treatment, which was mediated by TGF-βR expression in NPCs. Overexpression of smad3 induces $p27^{kip1}$ upregulation in the chick spinal cord (Garcia-Campmany & Marti, 2007). Therefore, it is likely that TGF-β1 action, upstream of $p27^{kip1}$, is related to smad3 translocation, which, in turn, would be followed by elevated NeuroD expression, resulting in neuronal differentiation (Fig. 7).

Following DFO treatment, the percentage of cells with smad3 translocation to the nucleus was comparable to observations made with 200 pg/mL TGF-β1 (as detected by ELISA). Although translocation of DFO-induced cells was relatively low, 200 pg/mL TGF-β1 should be sufficient to induce neurogenesis; a similar amount of translocation was induced with a higher dose of TGF-β1 (1 or 10 ng/mL) in our preliminary data.

TGF-β1 enhanced $p27^{kip1}$ expression and neuronal differentiation from NPCs

Transforming growth factor-β1 is expressed in proliferative zones and the cortical plate in developing rat cortex between E16 and post-natal day 30 (Miller, 2003), indicating involvement in cell proliferation and migration (Siegenthaler & Miller, 2004, 2005). Increased neuronal cell death and microgliosis have been observed in TGF-β1 knockout mice (Brionne *et al.*, 2003). In addition, TGF-β1 enhances neurogenesis in neural crest-derived progenitor cells (Hagedorn *et al.*, 2000) as well as adult hippocampal NPCs (Battista *et al.*, 2006). Pro-neurogenic effects of TGF-β1 in microglia-activated situations have also been reported

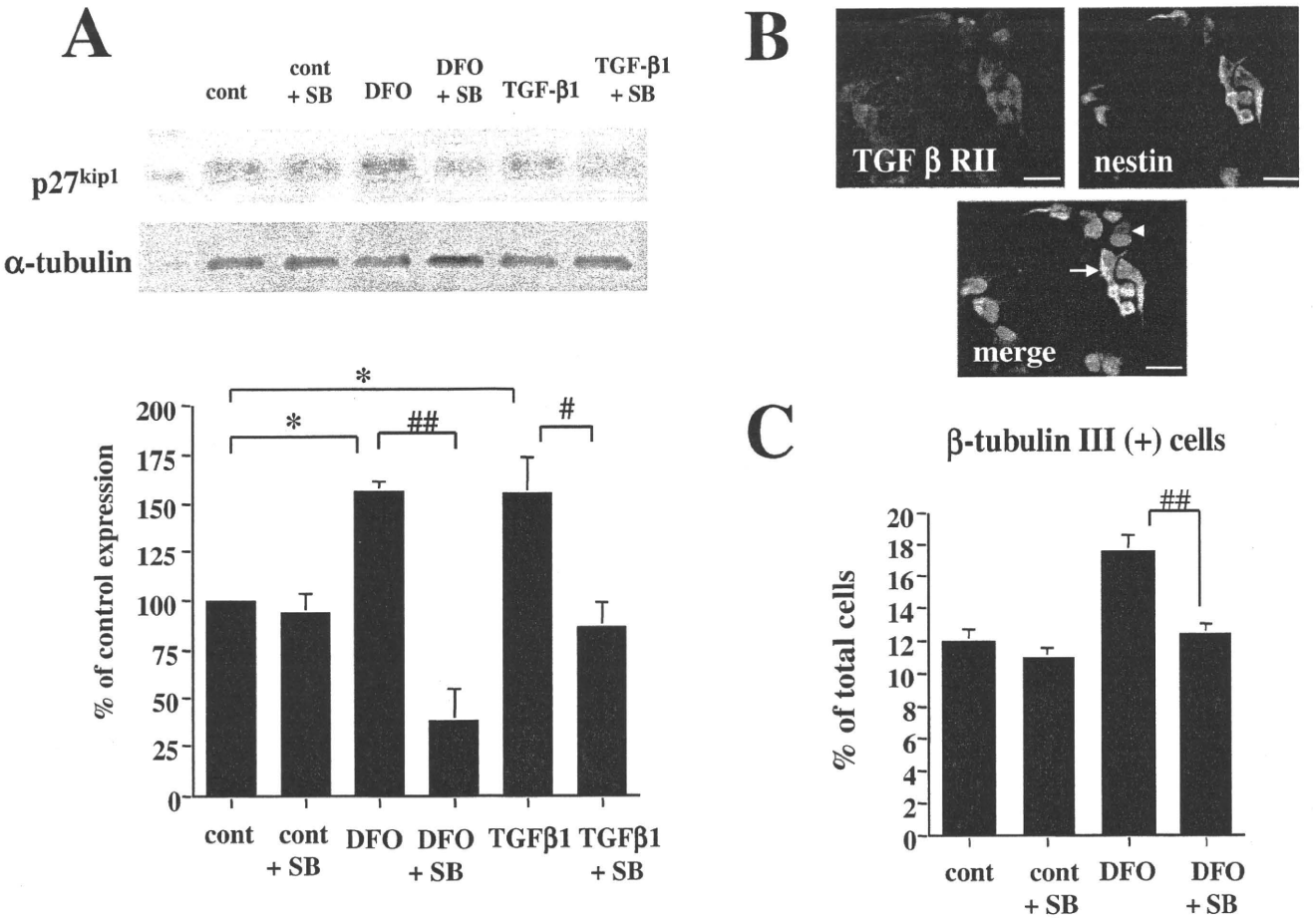

FIG. 5. Enhanced expression of $p27^{kip1}$ after DFO treatment is mediated by TGF-β signaling. (A) A TGF-β1R type I blocker, SB, was applied to neurospheres after DFO treatment, followed by detection of $p27^{kip1}$ proteins by western blot analysis (upper); quantification of $p27^{kip1}$ protein is shown in the lower graph. DFO-induced $p27^{kip1}$ expression ($n = 3$) was significantly inhibited by TGF-βR type I inhibition. The intensity of 27^{kip1} protein in each group was normalized to that of α-tubulin. (B) Expression of TGF-βR type II (TGF-βRII) and nestin was determined by double immunocytochemistry, along with DAPI nuclear staining. The colors (TGF-βRII, red; nestin, green; DAPI, blue) were merged (lower panel), showing expression of TGF-βRII in both nestin-positive (arrow) and nestin-negative (arrowhead) cells. (C) Enhanced number of β-tubulin III-positive cells by DFO was significantly decreased to the control (cont) level with SB administration ($n = 3$, $P < 0.01$). $^{*}P < 0.05$ as compared with control. $^{\#\#}P < 0.01$ for comparison between DFO and DFO + Ros, and $^{\#}P < 0.05$ for comparison between TGFβ1 and TGFβ1 + SB.

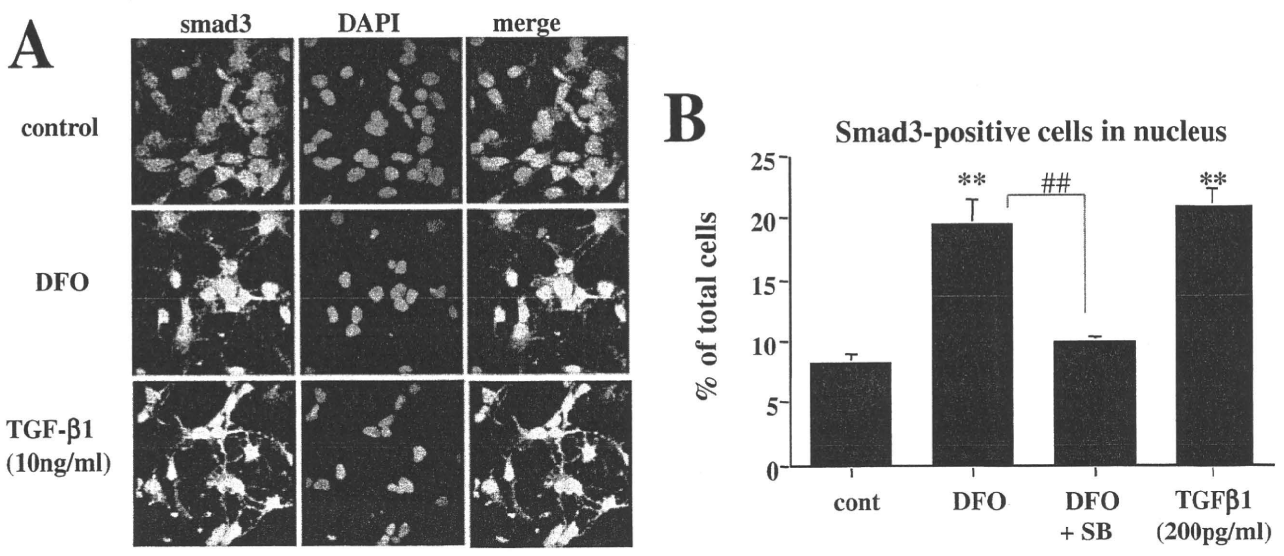

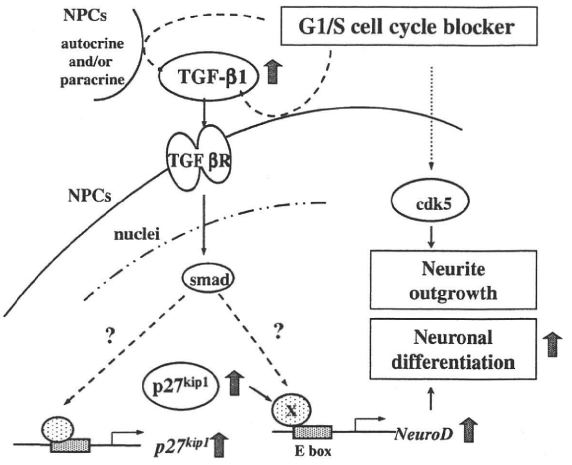

FIG. 7. Hypothesis of neuronal differentiation in NPCs after cell cycle arrest in G1/S-phase. The mechanism of enhanced neuronal differentiation after cell cycle arrest in G1/S-phase is depicted in the schema, which is based on data from the present study as well as previous data (Kim *et al.*, 2006). As for neuronal differentiation, G1/S-phase cell cycle blockers induce TGF-β1 expression in neurospheres in an autocrine and/or paracrine manner; TGF-β1 signaling is subsequently activated via the TGF-βR, thereby inducing smad3 translocation from the cytoplasm to the nucleus. The NeuroD promoter might be activated by smad3 via two pathways: (i) direct binding of smad3 to the NeuroD promoter mediated by factor X (neurogenin, etc.) or (ii) an indirect pathway via $p27^{kip1}$ protein, where smad3 expression correlates to enhanced $p27^{kip1}$ promoter activity. Finally, enhanced expression of NeuroD results in neuronal differentiation of NPCs. However, neurite outgrowth by a cell cycle blocker (DFO) is mediated by cdk5, giving the notion that this mechanism might be specific for some G1/S-phase cell cycle inhibitors and that the mechanism of neurite outgrowth by Aph is mediated by an unknown signal.

(Battista *et al.*, 2006). Therefore, TGF-β1 seems to be an important key molecule in neuronal development.

We clearly demonstrate in the present study that G1/S-phase cell cycle arrest upregulates TGF-β1 expression in NPCs. $p27^{kip1}$ transfection of neurospheres results in increased neurogenesis and activation of neurogenin-1 is subsequent to $p27^{kip1}$ elevation as we reported previously (Kim *et al.*, 2006). Therefore, $p27^{kip1}$ activation, downstream of TGF-β1 expression, is probably the cause of increased neurogenesis. Furthermore, the present results demonstrating that G1/S-phase cell cycle arrest upregulates TGF-β1 expression in NPCs, followed by increased neuronal differentiation via $p27^{kip1}$ activation, might suggest the possibility that any substances that are able to trigger G1/S-phase cell cycle arrest would also enhance neuronal differentiation during development.

DFO treatment alone is not sufficient for DAergic differentiation from neurospheres

Transforming growth factor-β2 and -β3 are expressed in E12 rat midbrain floor, and TGF-β3 has been particularly implicated in the development of midbrain dopaminergic (DAergic) neurons. In addition, these molecules display synergistic effects with sonic hedgehog (Farkas *et al.*, 2003; Zhang *et al.*, 2007). In the present study, there was no difference in TGF-β2 and -β3 levels between DFO-treated and control groups, which suggests that DFO treatment alone for 72 h is not sufficient to induce expression of factors that induce DAergic differentiation, such as TGF-β2 and -β3. Nevertheless, the possibility of DAergic expression in cells treated with DFO for longer periods of differentiation time cannot be excluded. Other factors that possess trophic activity for DAergic differentiation might be required to obtain DA neurons after DFO administration. We have reported that cytokines and trophic factors, such as pleiotrophin, IL1-β and LIF, which are enhanced in the DA-depleted striatum, promote induction of DA neurons in mouse embryonic stem cell-derived NPCs, relating to elevated hypoxia-inducible factor 1α expression (Hida *et al.*, 2003; Jung *et al.*, 2004; Kim *et al.*, 2008). Treatment with neurotrophic factors and cytokines, such as glial cell line-derived neurotrophic factor (GDNF), BDNF and pleiotrophin, combined with cell cycle regulation, should also be taken into consideration for further studies of DA differentiation.

Neurogenin-2 stabilizes $p27^{kip1}$ induction of neuronal differentiation by interacting with the N-terminal portion of the protein (Nguyen *et al.*, 2006). As synergistic actions between neurogenin-2 and Nurr1 have been reported to induce DA differentiation of NPCs (Andersson *et al.*, 2006), in the future it will be necessary to characterize the extrinsic signals that induce Nurr1.

Cdk5-mediated neurite outgrowth after DFO treatment

Cdk5 has been shown to play an important role in neurite length during neuronal differentiation (Nikolic *et al.*, 1996; Smith *et al.*, 2001) and has also been reported to associate with neuronal migration stabilizing $p27^{kip1}$ protein. Furthermore, the influence of cdk5 on neuronal survival through Bcl-2 phosphorylation has recently been reported (Cheung *et al.*, 2008). It is possible that the decreased number of neurons, through cdk5 inhibition (Ros), is related to inhibition of $p27^{kip1}$ stabilization or Bcl-2 phosphorylation. However, the present study was not able to detect a relationship between cdk5 and $p27^{kip1}$.

The DFO promoted neurite outgrowth, compared with the control cultures, and was related to cdk5 mRNA enhancement. However, TGF-β1 administration did not induce cdk5 mRNA expression in NPCs or alter neurite outgrowth but rather increased β-tubulin III-positive cells after 72 h of treatment. Therefore, the results suggest that cdk5 is involved in neurite outgrowth following cell cycle arrest, independent of TGF-β1 signaling. Further investigations are required to determine microtubule organization after TGF-β1 signaling.

Results from the present study are not able to explain the enhanced cdk5-only expression after DFO treatment, especially because the cdk5 co-activators, p35 and p39, were not altered by either DFO or Aph treatment. However, it is plausible that the DFO-induced signal is, at least in part, different from Aph, although the induction signal for TGF-β1 seems to be similar in both treatments.

FIG. 6. Nuclear translocation of smad3 by DFO treatment. (A) Following DFO treatment, cells were differentiated for 24 h and processed for immunocytochemistry using anti-smad3 antibody and DAPI. Localization of smad3 protein was observed primarily in the cytoplasm of control cultures (upper panels), whereas it was mainly detected in the nuclei of 10 ng/mL TGF-β1-treated cells (lower panels). Treatment with DFO induced translocation of smad3 to the nucleus at 24 h after differentiation. (B) There were more smad3-positive cells with nuclear localization in DFO-treated cells compared with control (cont) cells. Addition of SB to DFO-treated NPCs significantly decreased the percentage of smad3-positive cells with nuclear staining. Note that the addition of 200 pg/mL TGF-β1 was at a similar level as in the DFO treatment and induced translocation to the nucleus that was similar to DFO treatment. $^{**}P < 0.01$ as compared to control. $^{\#\#}P < 0.01$ for comaprison between DFO and DFO+Ros.

Probable merits of cell cycle inhibition for neural transplantation

Transforming growth factor-β1 exhibits protective effects on cell survival following the administration of various toxins and injuries to the central nervous system (Zhu *et al.*, 2002). Importantly, TGF-β1 is required as a cofactor for GDNF neuroprotective action (Schober *et al.*, 1999). TGF-β1 was also enhanced in the striatum of 1-methyl-4-phenyl-1,2,3,6-tetrahydropyrimide-lesioned mice and was essential for GDNF protection of DA neurons (Schober *et al.*, 2007). TGF-β1 upregulation in NPCs after DFO treatment suggests that TGF-β1 might be useful in the treatment of Parkinson's disease, with regard to neuronal differentiation and cell survival.

Acknowledgements

This work was supported by a Grant-in-Aid for Scientific Research on Priority Area (C) (no. 16500203 and no. 20500160 to H.H.) from the Japan Society for the Promotion of Science (JSPS) and by The Project of Realization for Regenerative Medicine (H.H.) from The Ministry of Education, Culture, Sports, Science and Technology (MECSST) and also supported by grants (H.H.) from Ajinomoto KK and Japan Brain Foundation.

Abbreviations

Aph, aphidicolin; cdk, cyclin-dependent kinase; DA, dopaminergic; DAPI, 4′,6-Diamidino-2-phenylindole; DFO, deferoxamine; E, embryonic day; GDNF, glial cell line-derived neurotrophic factor; MAP-2, microtubule-associated protein-2; NPC, neural stem/progenitor cell; PBS, phosphate-buffered saline; PCR, polymerase chain reaction; Ros, roscovitine; SB, SB-505124; TGF, transforming growth factor; TGF-βR, transforming growth factor-β receptor.

References

Andersson, E., Tryggvason, U., Deng, Q., Frilin, S., Alekseenko, Z., Robert, B., Perlmann, T. & Ericson, J. (2006) Identification of intrinsic determinants of midbrain dopamine neurons. *Cell*, **124**, 393–405.

Andersson, E.K., Irvin, D.K., Absjo, J. & Parmar, M. (2007) Ngn2 and Nurr1 act in synergy to induce midbrain dopaminergic neurons from expanded neural stem and progenitor cells. *Exp. Cell Res.*, **313**, 1172–1180.

Battista, D., Ferrari, C.C., Gage, F.H. & Pitossi, F.J. (2006) Neurogenic niche modulation by activated microglia: transforming growth factor beta increases neurogenesis in the adult dentate gyrus. *Eur. J. Neurosci.*, **23**, 83–93.

Bouchard, C., Fridman, W.H. & Sautes, C. (1997) Effect of TGF-beta1 on cell cycle regulatory proteins in LPS-stimulated normal mouse B lymphocytes. *J. Immunol.*, **159**, 4155–4164.

Brionne, T.C., Tesseur, I., Masliah, E. & Wyss-Coray, T. (2003) Loss of TGF-beta 1 leads to increased neuronal cell death and microgliosis in mouse brain. *Neuron*, **40**, 1133–1145.

Bull, N.D. & Bartlett, P.F. (2005) The adult mouse hippocampal progenitor is neurogenic but not a stem cell. *J. Neurosci.*, **25**, 10815–10821.

Carruthers, S., Mason, J. & Papalopulu, N. (2003) Depletion of the cell-cycle inhibitor p27(Xic1) impairs neuronal differentiation and increases the number of ElrC(+) progenitor cells in *Xenopus tropicalis*. *Mech. Dev.*, **120**, 607–616.

Casaccia-Bonnefil, P., Hardy, R.J., Teng, K.K., Levine, J.M., Koff, A. & Chao, M.V. (1999) Loss of p27Kip1 function results in increased proliferative capacity of oligodendrocyte progenitors but unaltered timing of differentiation. *Development*, **126**, 4027–4037.

Cheung, Z.H., Gong, K. & Ip, N.Y. (2008) Cyclin-dependent kinase 5 supports neuronal survival through phsphorylation of Bcl-2. *J. Neurosci.*, **28**, 4872–4877.

Cunningham, J.J. & Roussel, M. (2001) Cyclin-dependent kinase inhibitors in the development of the central nervous system. *Cell Growth Differ.*, **12**, 387–396.

ten Dijke, P. & Hill, C.S. (2004) New insights into TGF-beta-Smad signalling. *Trends Biochem. Sci.*, **29**, 265–273.

Dyer, M.A. & Cepko, C.L. (2001) Regulating proliferation during retinal development. *Nat. Rev.*, **2**, 333–342.

Farkas, L.M., Dunker, N., Roussa, E., Unsicker, K. & Krieglstein, K. (2003) Transforming growth factor-beta(s) are essential for the development of midbrain dopaminergic neurons in vitro and in vivo. *J. Neurosci.*, **23**, 5178–5186.

Garcia-Campmany, L. & Marti, E. (2007) The TGFbeta intracellular effector Smad3 regulates neuronal differentiation and cell fate specification in the developing spinal cord. *Development*, **134**, 65–75.

Gritti, A., Parati, E.A., Cova, L., Frolichsthal, P., Galli, R., Wanke, E., Faravelli, L., Morassutti, D.J., Roisen, F., Nickel, D.D. & Vescovi, A.L. (1996) Multipotential stem cells from the adult mouse brain proliferate and self-renew in response to basic fibroblast growth factor. *J. Neurosci.*, **16**, 1091–1100.

Hagedorn, L., Floris, J., Suter, U. & Sommer, L. (2000) Autonomic neurogenesis and apoptosis are altenative fates of progenitor cell communities induced by TGFbeta. *Dev. Biol.*, **228**, 55–72.

Hida, H., Jung, C.G., Wu, C.Z., Kim, H.J., Kodama, Y., Masuda, T. & Nishino, H. (2003) Pleiotrophin exhibits a trophic effect on survival of dopaminergic neurons in vitro. *Eur. J. Neurosci.*, **17**, 2127–2134.

Joseph, B., Wallen-Mackenzie, A., Benoit, G., Murata, T., Joodmardi, E., Okret, S. & Perlmann, T. (2003) p57(Kip2) cooperates with Nurr1 in developing dopamine cells. *Proc. Natl Acad. Sci. USA*, **100**, 15619–15624.

Jung, C.G., Hida, H., Nakahira, K., Ikenaka, K., Kim, H.J. & Nishino, H. (2004) Pleiotrophin mRNA is highly expressed in neural stem (progenitor) cells of mouse ventral mesencephalon and the product promotes production of dopaminergic neurons from embryonic stem cell-derived nestin-positive cells. *FASEB J.*, **18**, 1237–1239.

Kawauchi, T., Chihama, K., Nabeshima, Y. & Hoshino, M. (2006) Cdk5 phosphorylates and stabilizes p27kip1 contributing to actin organization and cortical neuronal migration. *Nat. Cell Biol.*, **8**, 17–26.

Kim, H.J., Hida, H., Jung, C.G., Miura, Y. & Nishino, H. (2006) Treatment with deferoxamine increases neurons from neural stem/progenitor cells. *Brain Res.*, **1092**, 1–15.

Kim, T.S., Misumi, S., Jung, C.G., Masuda, T., Isobe, Y., Furuyama, F., Nishino, H. & Hida, H. (2008) Increase in dopaminergic neurons from mouse embryonic stem cell-derived neural progenitor/stem cells is mediated by hypoxia inducible factor-1α. *J. Neurosci. Res.*, **86**, 2253–2262.

Ko, T.C., Yu, W., Sakai, T., Sheng, H., Shao, J., Beauchamp, R.D. & Thompson, E.A. (1998) TGF-beta1 effects on proliferation of rat intestinal epithelial cells are due to inhibition of cyclin D1 expression. *Oncogene*, **16**, 3445–3454.

Levine, E.M., Close, J., Fero, M., Ostrovsky, A. & Reh, T.A. (2000) p27(Kip1) regulates cell cycle withdrawal of late multipotent progenitor cells in the mammalian retina. *Dev. Biol.*, **219**, 299–314.

Lim, M.S., Nam, S.H., Kim, S.J., Kang, S.Y., Lee, Y.S. & Kang, K.S. (2007) Signaling pathways of the early differentiation of neural stem cells by neurotrophin-3. *Biochem. Biophys. Res. Commun.*, **357**, 903–909.

Massague, J., Seoane, J. & Wotton, D. (2005) Smad transcription factors. *Genes Dev.*, **19**, 2783–2810.

Miller, M.W. (2003) Expression of transforming growth factor-beta in developing rat cerebral cortex: effects of prenatal exposure to ethanol. *J. Comp. Neurol.*, **460**, 410–424.

Mitsuhashi, T., Aoki, Y., Eksioglu, Y.Z., Takahashi, T., Bhide, P.G., Reeves, S.A. & Caviness, V.S. Jr (2001) Overexpression of p27Kip1 lengthens the G1 phase in a mouse model that targets inducible gene expression to central nervous system progenitor cells. *Proc. Natl Acad. Sci. USA*, **98**, 6435–6440.

Nguyen, L., Besson, A., Heng, J.I., Schuurmans, C., Teboul, L., Parras, C., Philpott, A., Roberts, J.M. & Guillemot, F. (2006) p27kip1 independently promotes neuronal differentiation and migration in the cerebral cortex. *Genes Dev.*, **20**, 1511–1524.

Nikolic, M., Dudek, H., Kwon, Y.T., Ramos, Y.F. & Tsai, L.H. (1996) The cdk5/p35 kinase is essential for neurite outgrowth during neuronal differentiation. *Genes Dev.*, **10**, 816–825.

Ohnuma, S. & Harris, W.A. (2003) Neurogenesis and the cell cycle. *Neuron*, **40**, 199–208.

Ohnuma, S., Philpott, A., Wang, K., Holt, C.E. & Harris, W.A. (1999) p27Xic1, a CDK inhibitor, promotes the determination of glial cells in Xenopus retiana. *Cell*, **99**, 499–510.

Ohnuma, S., Philpott, A. & Harris, W.A. (2001) Cell cycle and cell fate in the nervous system. *Curr. Opin. Neurobiol.*, **11**, 66–73.

Polyak, K., Kato, J.Y., Solomon, M.J., Sherr, C.J., Massague, J., Roberts, J.M. & Koff, A. (1994) p27Kip1, a cyclin-Cdk inhibitor, links transforming growth factor-beta and contact inhibition to cell cycle arrest. *Genes Dev.*, **8**, 9–22.

Reynolds, B.A. & Weiss, S. (1992) Generation of neurons and astrocytes from isolated cells of the adult mammalian central nervous system. *Science*, **255**, 1707–1710.

Roussa, E. & Krieglstein, K. (2004) Induction and specification of midbrain dopaminergic cells: focus on SHH, FGF8, and TGF-beta. *Cell Tissue Res.*, **318**, 23–33.

Schober, A., Hertel, R., Arumae, U., Farkas, L., Jaszai, J., Krieglstein, K., Saarma, M. & Unsicker, K. (1999) Glial cell line-derived neurotrophic factor rescues target-deprived sympathetic spinal cord neurons but requires transforming growth factor-beta as cofactor in vivo. *J. Neurosci.*, **19**, 2008–2015.

Schober, A., Peterziel, H., von Bartheld, C.S., Simon, H., Krieglstein, K. & Unsicker, K. (2007) GDNF applied to the MPTP-lesioned nigrostriatal system requires TGF-β for its neuroprotective action. *Neurobiol. Dis.*, **25**, 378–391.

Siegenthaler, J.A. & Miller, M.W. (2004) Transforming growth factor beta1 modulates cell migration in rat cortex: effects of ethanol. *Cereb. Cortex*, **14**, 791–802.

Siegenthaler, J.A. & Miller, M.W. (2005) Transforming growth factor beta 1 promotes cell cycle exit through the cyclin-dependent kinase inhibitor p21 in the developing cerebral cortex. *J. Neurosci.*, **25**, 8627–8636.

Smith, D.S., Greer, P.L. & Tsai, L.H. (2001) Cdk5 on the brain. *Cell Growth Differ.*, **12**, 277–283.

Storch, A., Paul, G., Csete, M., Boehm, B.O., Carvey, P.M., Kupsch, A. & Schwarz, J. (2001) Long-term proliferation and dopaminergic differentiation of human mesencephalic neural precursor cells. *Exp. Neurol.*, **170**, 317–325.

Sun, Y., Nadal-Vicens, M., Misono, S., Lin, M.Z., Zubiaga, A., Hua, X., Fan, G. & Greenberg, M.E. (2001) Neurogenin promotes neurogenesis and inhibits glial differentiation by independent mechanisms. *Cell*, **104**, 365–376.

Turnley, A.M., Faux, C.H., Rietze, R.L., Coonan, J.R. & Bartlett, P.F. (2002) Suppressor of cytokine signaling 2 regulates neuronal differentiation by inhibiting growth hormone signaling. *Nat. Neurosci.*, **5**, 1155–1162.

Vernon, A.E., Devine, C. & Philpott, A. (2005) The cdk inhibitor p27Xic1 is required for differentiation of primary neurones in Xenopus. *Development*, **130**, 85–92.

Williams, B.P., Park, J.K., Alberta, J.A., Muhlebach, S.G., Hwang, G.Y., Roberts, T.M. & Stiles, C.D. (1997) A PDGF-regulated immediate early gene response initiates neuronal differentiation in ventricular zone progenitor cells. *Neuron*, **18**, 553–562.

Wolfraim, L.A., Walz, T.M., James, Z., Fernandez, T. & Letterio, J.J. (2004) p21Cip1 and p27Kip1 act in synergy to alter the sensitivity of naive T cells to TGF-beta-mediated G1 arrest through modulation of IL-2 responsiveness. *J. Immunol.*, **173**, 3093–3102.

Wong, G., Goldshmit, Y. & Turnley, A.M. (2004) Interferon-gamma but not TNF alpha promotes neuronal differentiation and neurite outgrowth of murine adult neural stem cells. *Exp. Neurol.*, **187**, 171–177.

Yang, M., Stull, N.D., Berk, M.A., Snyder, E.Y. & Iacovitti, L. (2002) Neural stem cells spontaneously express dopaminergic traits after transplantation into the intact or 6-hydroxydopamine-lesioned rat. *Exp. Neurol.*, **177**, 50–60.

Yoo, Y.D., Choi, J.Y., Lee, S.J., Kim, J.S., Min, B.R., Lee, Y.I. & Kang, Y.K. (1999) TGF-beta-induced cell-cycle arrest through the p21(WAF1/CIP1)-G1 cyclin/Cdks-p130 pathway in gastric-carcinoma cells. *Int. J. Cancer*, **83**, 512–517.

Yoon, G., Kim, H.J., Yoon, Y.S., Cho, H., Lim, I.K. & Lee, J.H. (2002) Iron chelation-induced senescence-like growth arrest in hepatocyte cell lines: association of transforming growth factor beta1 (TGF-beta1)-mediated p27Kip1 expression. *Biochem. J.*, **366**, 613–621.

Zhang, J., Pho, V., Bonasera, S.J., Holtzman, J., Tang, A.T., Hellmuth, J., Tang, S., Janak, P.H., Tecott, L.H. & Huang, E.J. (2007) Essential function of HIPK2 in TGFbeta-dependent survival of midbrain dopamine neurons. *Nat. Neurosci.*, **10**, 77–86.

Zhu, Y., Yang, G.Y., Ahlemeyer, B., Pang, L., Che, X.M., Culmsee, C., Klumpp, S. & Krieglstein, J. (2002) Transforming growth factor-beta 1 increases bad phosphorylation and protects neurons against damage. *J. Neurosci.*, **22**, 3898–3909.

Infection of Myeloid Dendritic Cells with *Listeria monocytogenes* Leads to the Suppression of T Cell Function by Multiple Inhibitory Mechanisms[1]

Alexey Popov,[2]* Julia Driesen,[2]* Zeinab Abdullah,[†] Claudia Wickenhauser,[‡] Marc Beyer,* Svenja Debey-Pascher,* Tomo Saric,[§] Silke Kummer,[‡] Osamu Takikawa,[¶] Eugen Domann,[‖] Trinad Chakraborty,[‖] Martin Krönke,[†] Olaf Utermöhlen,[†] and Joachim L. Schultze[3]*

Myeloid dendritic cells (DC) and macrophages play an important role in pathogen sensing and antimicrobial defense. In this study we provide evidence that myeloid DC respond to infection with *Listeria monocytogenes* with simultaneous induction of multiple stimulatory and inhibitory molecules. However, the overall impact of infected DC during T cell encounter results in suppression of T cell activation, indicating that inhibitory pathways functionally predominate. Inhibitory activity of infected DC is effected mainly by IL-10 and cyclooxygenase 2-mediated mechanisms, with soluble CD25 acting as an IL-2 scavenger as well as by the products of tryptophan catabolism. These inhibitory pathways are strictly TNF-dependent. In addition to direct infection, DC bearing this regulatory phenotype can be induced in vitro by a combination of signals including TNF, TLR2, and prostaglandin receptor ligation and by supernatants derived from the infected cells. Both infection-associated DC and other in vitro-induced regulatory DC are characterized by increased resistance to infection and enhanced bactericidal activity. Furthermore, myeloid DC expressing multiple regulatory molecules are identified in vivo in granuloma during listeriosis and tuberculosis. Based on the in vivo findings and the study of in vitro models, we propose that in granulomatous infections regulatory DC may possess dual function evolved to protect the host from disseminating infection via inhibition of granuloma destruction by T cells and control of pathogen spreading. *The Journal of Immunology*, 2008, 181: 4976–4988.

Phagocytic cells play an important role in the defense against infectious pathogens including intracellular bacteria, for example, *Listeria monocytogenes* (*L.m.*)[4] (1) and *Mycobacterium tuberculosis* (2). Macrophages and neutrophils play a major role during early immune responses against these intracellular pathogens (3, 4), and yet, for a complete clearance of infection, an efficient adaptive immune response involving dendritic cells (DC) is required (1). As shown in listeriosis, DC are involved in pathogen elimination (5) and induction of Ag-specific $CD8^+$ T cell responses (6). In vitro studies demonstrated an induction of costimulatory molecules on human DC after *Listeria* infection (7, 8). However, there is also evidence that macrophages and DC infected by intracellular bacteria, viruses, and parasites can acquire regulatory phenotype and exert inhibitory function (9–12). Infection of human DC with *L.m.* leads to up-regulation of the immune inhibitory enzyme IDO, a key enzyme of tryptophan metabolism (10). Moreover, in vivo, an increase in DC numbers resulted in impaired protective immunity to subsequent infection of mice with *L.m.* (6), suggesting that DC-mediated inhibitory mechanisms might play a role in host-pathogen interaction.

During recent years, it has been suggested that DC are not only the most stimulatory cells for the induction of Ag-specific T cell responses (13), but that they are also capable of inhibiting T cell activation or even inducing T cell tolerance (14, 15). Numerous mechanisms have been linked to the phenotype of such cells, which are termed "tolerogenic" or "regulatory" DC (15–17). Down-regulation of costimulatory molecules (18) and stimulatory cytokines such as IL-12 (19), induction of coinhibitory molecules (e.g., PDL1 or TGF-β) (20, 21), as well as enzymatic mechanisms such as tryptophan catabolism (22, 23) have been identified as major inhibitory effectors of regulatory DC. The detrimental effect of such DC on Ag-specific immune responses is best illustrated in malignant disease (24), while their utility is explored in induction of tolerance in organ transplantation (15).

In infectious diseases, however, the existence of regulatory DC does not seem to be intuitively productive. We therefore examined regulation, expression, and function of immunoregulatory pathways in relation to granulomatous infection in vivo and in vitro primarily using *L.m.* and human DC as a model system. Under these conditions regulatory myeloid DC and macrophages seem to play a dual role within granuloma by impairing T cell-mediated

*Genomics and Immunoregulation, Institute for Life and Medical Sciences, University of Bonn, Bonn, Germany; [†]Institute for Medical Microbiology, Immunology and Hygiene, [‡]Institute for Pathology, and [§]Institute for Neurophysiology, University of Cologne, Cologne, Germany; [¶]National Institute for Longevity Sciences, National Center for Geriatrics and Gerontology, Obu, Aichi, Japan; and [‖]Institute of Medical Microbiology, University of Giessen, Giessen, Germany

Received for publication March 28, 2008. Accepted for publication August 1, 2008.

The costs of publication of this article were defrayed in part by the payment of page charges. This article must therefore be hereby marked *advertisement* in accordance with 18 U.S.C. Section 1734 solely to indicate this fact.

[1] This work was supported by a Sofja Kovalevskaja Award from the Alexander von Humboldt Foundation (to J.L.S.), a Köln Fortune Grant (to J.L.S. and T.S.), grants of the Bundesministerium fuer Bildung and Forschung NGFN 01GS0111 (to T.C.) and NGFN N1K3-S24T27 (to J.L.S.) and grants from the Deutsche Forschungsgemeinschaft SFB704 (to J.L.S.), SFB589 (to C.W.), and SFB670 (to M.K. and O.U.).

[2] A.P. and J.D. contributed equally to this work.

[3] Address correspondence and reprint requests to Dr. Joachim L. Schultze, Laboratory for Genomics and Immunoregulation, Program Unit Molecular Immune and Cell Biology, LIMES (Life and Medical Sciences Bonn), University of Bonn, Karlrobert-Kreitenstrasse 13, D-53115 Bonn, Germany. E-mail address: j.schultze@uni-bonn.de

[4] Abbreviations used in this paper: *L.m.*, *Listeria monocytogenes*; COX-2, cyclooxygenase 2; DC, dendritic cells; DCreg, regulatory DC; immDC, immature DC; infDC, infected DC; matDC, mature DC; mo-DC, monocyte-derived DC; Pam_3, Pam_3Cys-Ser-$(Lys)_4$.trihydrochloride; PGE_2, prostaglandin E_2; PGE_2-DC, mature inhibitory DC stimulated with PGE_2; rhIL-2, recombinant human IL-2; sCD25, soluble CD25.

immune responses against the infected cells in the granuloma while at the same time inhibiting pathogen growth. Altogether, the induction of regulatory DC and macrophages especially in granulomatous infections might be favorable to the host.

Materials and Methods

Peripheral blood samples

Blood samples were collected from healthy blood donors at the Center for Transfusion Medicine after informed written consent was obtained. All experiments were approved by the University of Cologne Institutional Review Board.

Immunohistochemistry and immunofluorescence

Lymph node specimens from patients with clinically and serologically confirmed cervicoglandular listeriosis and tuberculosis were obtained from the Institute of Pathology (University of Cologne). As a control, tonsils and lymph nodes of uninfected patients were used. Immunohistochemical and immunofluorescence analyses of paraffin-embedded tissue samples were performed with Abs for S100, CD4, CD8, and CD83 (DakoCytomation), CD11c and CD25 (NovoCastra), CD56 (Zytomed), IDO (Serotec), cyclooxygenase 2 (COX-2) (IBL International), and FoxP3 (eBioscience) as described before (10).

Flow cytometry

Flow cytometry (FACSCanto, BD Biosciences) was performed using the following mAbs: CD3, CD11c, CD14, CD16, CD19, CD25, CD54, CD56, and anti-HLA-DR (BD Biosciences), CD11b, CD40, CD80, and CD86 (BD Pharmingen), anti-TNF-RI, anti-TNF-RII, and CCR7 (R&D Systems), CD58 and CD83 (Immunotech), and CD68 (Serotec) with appropriate isotype controls. Intracellular staining for IDO (monoclonal mouse anti-human IDO Ab) (25) and IFN-γ (IFN-γ-PE, Immunotech) was performed using Cytofix/Cytoperm Plus kit with GolgiStop (BD Biosciences) according to the manufacturer's instructions. All flow cytometric data were assessed with the BD CellQuest 3.3 software (BD Biosciences).

In vitro generation of monocyte-derived DC and macrophages

DC were generated according to standard protocols, as previously described (10, 26). For maturation, DC were incubated with TNF (Sigma-Aldrich), anti-CD40 mAb (BD Pharmingen) with or without prostaglandin E_2 (PGE_2, Sigma-Aldrich), as previously described (26). For some experiments, DC were treated with TNF in combination with PGE_2 and Pam_3Cys-Ser-$(Lys)_4$.trihydrochloride (Pam_3, Axxora, 1 μg/ml), TNF and PGE_2, TNF and Pam_3, or incubated with LPS (Sigma-Aldrich, 1 μg/ml). Alternatively, 50% of supernatants derived from immature DC (immDC), TNF-matured DC (matDC), or infected DC (infDC) were added to allogeneic immDC or matDC, respectively. Additionally, immDC were incubated with matDC or infDC in a 0.4-μm polycarbonate transwell system (Nunc). Macrophages were generated from monocytes, as previously described (10).

Infection of cells with L.m.

Wild-type strain (EGD) of *L.m.* was processed as previously described (10). Heat-killed *Listeria* were obtained by incubating wild-type bacteria at 65°C for 1 h. Monocytes, DC, and macrophages were infected with FITC-labeled *Listeria* or incubated with heat-killed *Listeria* at multiplicity of infection of 10 and infection efficiency was controlled by flow cytometry as previously described (10). Following the infection phase, cells were recultivated in fresh medium; for prolonged cultures (>12 h), gentamicin (50 μg/ml, Sigma-Aldrich) was added. For some experiments, DC treated with heat-killed *Listeria* were pulsed with recombinant human IL-2 (rhIL-2, Chiron) 24 h after the treatment onset and supernatants were collected after additional 48 h for functional assays.

Neutralization experiments

Listeria-infected DC were incubated with appropriate neutralizing mAbs or inhibitors, as previously described (10). The following Abs were used: anti-TNF mAb (20 μg/ml, BD Pharmingen), clinically applied TNF-neutralizing Ab infliximab (0.001–10 μg/ml, Centocor), anti-IFN-γ mAb (0.1–1 μg/ml, BD Pharmingen), anti-IL-10 mAb (5 μg/ml, R&D Systems), and anti-TNF-RI and anti-TNF-RII mAbs (10–100 μg/ml). The COX-2 inhibitor rofecoxib (a gift of Drs. K. Schrör and J. Meyer-Kirchrath) was used at 1–10 μM.

RNA preparation, microarray hybridization, and data processing

Immature DC were harvested on day 7 and mature DC were harvested 72 h upon start of maturation. Infected and corresponding control monocyte-derived DC (mo-DC) were harvested 2, 4, 6, and 24 h after infection. RNA and cRNA preparation, microarray hybridization (HG-U133A, Affymetrix), data analysis, and visualization were performed as previously described (10, 26). Microarray data are accessible at the National Center for Biotechnology Information (NCBI) Gene Expression Omnibus (GEO) database (accession no. GSE9946 at http://www.ncbi.nlm.nih.gov/geo/query/acc.cgi?acc).

Quantitative real-time PCR

Quantitative analysis of real-time PCR was performed using LightCycler3 and RelQuant software, version 1.0 (Roche Diagnostics), as previously described (10). Primers used (Roche Diagnostics) included: *IL2RA* forward, ACTGCTCACGTTCATCATGG, reverse, GATCTCTGGCGGGTC ATC, Universal ProbeLibrary probe no. 13; *B2M* forward, TTCTGGCC TGGAGGCTAT, reverse, TCAGGAAATTTGACTTTCCATTC, Universal ProbeLibrary probe no. 42.

Western blotting

COX-2 expression was assessed by anti-COX-2 polyclonal Ab (IBL International) as previously described (10). Alternatively, Western blots for COX-2 or IDO (25) were performed on the LI-COR Odyssey System (LI-COR Biosciences) according to the manufacturer's instructions.

ELISA

Soluble CD25, IL-2, TNF, IL-10, and IFN-γ in cell supernatants were measured by sIL-2R, IL-2, IFN-γ, IL-10, and TNF-α Eli-Pair kits (Diaclone Research) according to the manufacturer's instructions. All samples were analyzed at least in duplicates.

Assessment of kynurenine levels by photometrical assay

Assessment of kynurenine levels in the supernatants was performed as previously described (10, 25). Samples were run in triplicates against a standard curve of L-kynurenine concentrations (Sigma-Aldrich).

Mixed leukocyte reaction

MLR was performed as previously described (26). Briefly, freshly isolated allogeneic $CD4^+$ T cells were labeled with CFSE and incubated with DC at different ratios. DC were either incubated for 24 h in 96-well plates before T cells were added or they were additionally washed before MLR for the assay to be performed in fresh medium. In some experiments, magnetic beads, coated with anti-CD3 mAb or with anti-CD3 and anti-CD28 mAbs (27) at ratios of 1:1 or 1:10 (beads/T cells) were added. Alternatively, CD3/CD28-activated T cells were incubated with matDC or infDC in a transwell system. To neutralize the suppressive effect of infected DC, 1-methyl-tryptophan (10 μM, Sigma Aldrich), anti-IL-10 mAb (10 μg/ml), rofecoxib (10 μM), and rhIL-2 (20 U/ml) were given separately or in combination. After 3 days of culture, T cell proliferation was assessed by flow cytometry.

Inhibition of T cell proliferation

To study the effect of DC-derived soluble factors on CD3/CD28-induced T cell proliferation, CFSE-labeled $CD4^+$ T cells were incubated with L-kynurenine (Sigma-Aldrich), IL-10 (R&D Systems), or PGE_2 in a range of concentrations in either RPMI 1640 (Invitrogen) or in tryptophan-free RPMI 1640 medium (BioWhittaker) for 3 days until T cell proliferation was assessed by flow cytometry. Alternatively, CD3/CD28-activated T cells were incubated with supernatants derived from matDC or infDC (in a dilution range from 1 to 100%). In some experiments, T cell proliferation was assessed by incorporation of BrdU (Roche Diagnostics): cells were pulsed with BrdU on day 2 of culture and harvested 24 h thereafter; subsequently, BrdU incorporation was assessed according to the manufacturer's instructions.

Assessment of proliferation and viability of CTLL-2 cells

The murine IL-2-dependent T cell line CTLL-2 was obtained from the American Type Culture Collection (TIB-214) and cultured in supernatants derived from DC supplemented with rhIL-2 as previously described (26). Cell proliferation was determined by cell counting and viability assessed by flow cytometry with propidium iodide (Sigma-Aldrich).

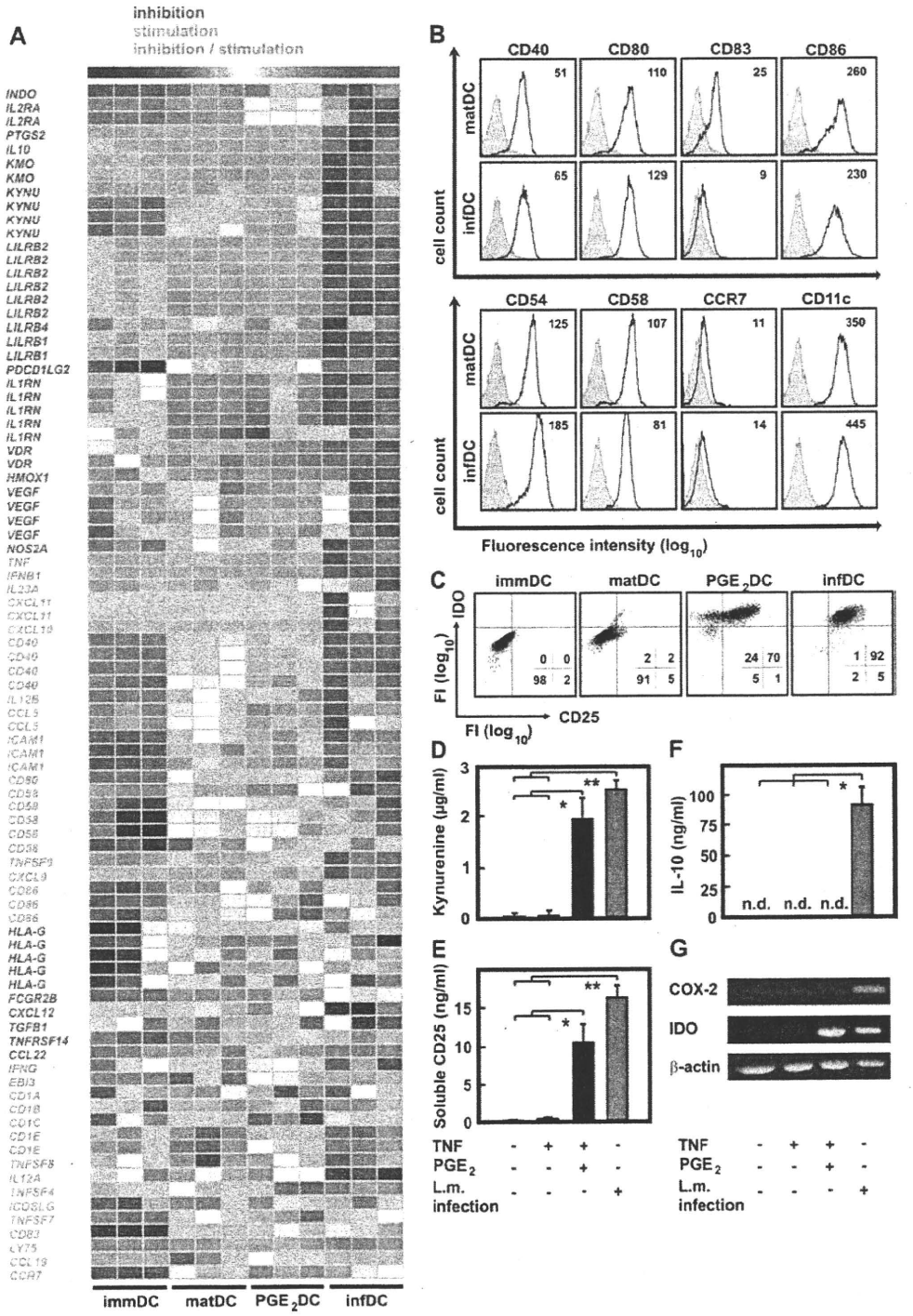

FIGURE 1. Induction of stimulatory and regulatory molecules during infection of human DC with *L.m.* DC were generated from monocytes as described in *Materials and Methods*. Asterisks highlight the statistically significant differences. *A*, Heat map displaying expression of genes associated with inhibitory or stimulatory function of DC. Average expression signals were obtained from microarray experiments and were standardized (Z score transformation) before visualization. Gene symbols for transcripts involved in stimulation or inhibition are differentially color-coded. Three independent DC cultures resulting in three array hybridizations were performed per DC subset and are shown in the heat map. *B*, Expression of activation markers, costimulatory molecules, and myeloid lineage marker CD11c by monocyte-derived DC either matured with TNF (matDC) or infected with *L.m.* (infDC) was studied by flow cytometry 24 h upon the start of maturation or infection, respectively. Isotype controls are shown as gray area underneath the thin line; expressionof specific Abs is reflected by thick black lines; mean fluorescence intensity values are shown in the right upper corner. One representative experiment of three is shown. *C*, Expression of CD25 (surface staining) and IDO (intracellular staining) by DC was assessed by flow cytometry (representative experiment, $n = 4$). Percentage of positive cells for each quadrant is shown in the right lower corner. *D*, Kynurenine accumulation in supernatants as a measure of IDO activity was assessed using a photometric assay (mean ± SD, $n = 4$). *, $p < 0.005$ and **, $p < 0.00005$. *E*, Secretion of soluble CD25 was assessed by ELISA (mean ± SD, $n = 4$). *, $p < 0.005$ and **, $p < 0.0005$. *F*, IL-10 secretion was assessed by ELISA (mean ± SD, $n = 4$). *, $p < 0.005$; n.d., not detectable. *G*, Protein expression of COX-2 and β-actin (as loading control) was assessed by Western blot. After stripping, the membrane was additionally incubated with IDO mAb. One representative experiment out of four is shown.

Assessment of L.m. *viability*

Immediately after infection, DC were lysed and the number of viable *Listeria* (initial bacterial burden) was determined in a CFU assay on blood agar. Consequently, bactericidal activity of DC was analyzed after various periods of time. Additionally, *L.m.* was incubated for 6 h in a tryptophan-free RPMI 1640 medium supplemented with different concentrations of L-tryptophan and L-kynurenine (Sigma Aldrich) and *Listeria* viability was controlled by CFU assay.

Statistical analysis

Statistical analysis was performed using R software package (version 2.3.0). To calculate statistical significance, a two-sample two-tailed t test was used. Comparisons with a p-value <0.05 were called statistically significant.

Results

Human DC express numerous stimulatory and inhibitory molecules upon infection with L.m.

We have recently demonstrated that infection of human DC with *L.m.* leads to the induction of the immunoinhibitory enzyme IDO (10), while in other studies *L.m.* infection was associated with a stimulatory DC phenotype (7, 8). To clarify this apparent discrepancy we performed detailed comparative microarray analysis on myeloid DC infected with *L.m.* (infDC) (10), mature inhibitory DC stimulated with prostaglandin E_2 (PGE_2-DC) and expressing IDO (26), mature stimulatory DC lacking the expression of IDO (matDC), and immDC. For presentation of differentially expressed transcripts associated with inhibitory or stimulatory DC function (reviewed in detail in Refs. 16, 17) expression values were standardized using Z score transformation at the probeset level and visualized as a heat map.

As shown in Fig. 1*A*, infDC are enriched for numerous transcripts associated with stimulatory as well as inhibitory DC function. Among inhibitory genes *PTGS2* (COX-2), *IL10* (IL-10), and *IL2RA* (CD25), enzymes of tryptophan catabolism and inhibitory Ig-like transcripts were most strongly induced in infDC (Fig. 1*A*). Furthermore, transcripts for TNF, IFN-β, and IL-23, which can exert antiinflammatory action (28), were up-regulated only in infDC. Stimulatory genes induced by infection included various chemokines, cell adhesion (*ICAM1* and *CD58*) and costimulatory molecules (*CD40*, *CD80*, *CD86*, and *TNFSF9*). However, other important stimulatory molecules, such as *CD83*, *CCR7*, *CCL19*, TNF superfamily members, and CD1 family molecules were only up-regulated in noninfected stimulatory matDC (Fig. 1*A*). Altogether, infDC present a rather specific transcriptional "signature" that distinguishes them from immDC, stimulatory matDC, and inhibitory PGE_2-DC: they simultaneously express numerous inhibitory as well as stimulatory molecules.

Assessment of surface receptor expression by flow cytometry demonstrated that infDC and stimulatory matDC expressed comparable amounts of costimulatory and adhesion molecules but differed in expression of CD83 (Fig. 1*B*). To corroborate transcriptional regulation of inhibitory molecules, expression of CD25, IL-10, and COX-2 was assessed using IDO as a control marker for regulatory DC (17). Cell-surface CD25 is up-regulated in virtually all infDC and is coexpressed with intracellular IDO, while only 70% of inhibitory PGE_2-DC expressed CD25 (Fig. 1*C*). ImmDC and matDC did not express CD25 and IDO. Supernatants from infDC contained significant amounts of kynurenine as a consequence of functional IDO expression (Fig. 1*D*). Moreover, infDC secreted large amounts of soluble CD25 (sCD25) (Fig. 1*E*). The onset of CD25 mRNA expression, as assessed by quantitative real-time PCR, was faster and the amount of secreted sCD25 after *L.m.* infection was higher (data not shown) as compared with PGE_2-DC (30). In contrast to CD25 and IDO, IL-10 and COX-2 were only induced by infDC but not by other DC subsets (Fig. 1, *F* and *G*). The kinetics of IL-10 secretion resembled that of sCD25 (data not shown). Altogether, infection of myeloid DC by *L.m.* induces stimulatory molecules together with numerous inhibitory pathways previously associated with regulatory DC function (16, 17).

Functional predominance of inhibitory pathways in infected DC

In light of expression of inhibitory and stimulatory molecules by infDC, we next studied the impact of infDC on T cell activation. First, the stimulatory capacity of infDC in comparison to other DC subsets was assessed in an allogeneic MLR using purified $CD4^+$ T cells and beads coated with low-dose anti-CD3 mAb, thus providing equal signal 1 for all conditions (27). Treatment of T cells with anti-CD3 beads alone did not induce T cell proliferation or T cell cytokine production (Fig. 2*A* and data not shown). Co-cultures of T cells and matDC in the presence of anti-CD3 beads induced significant T cell proliferation (Fig. 2*A*) comparable to beads coated with anti-CD3 and anti-CD28 Abs (Fig. 2*A*). However, when T cells were cocultured with DC without anti-CD3 beads, proliferation was very low (Fig. 2*A*), and therefore the following MLR experiments were performed with anti-CD3 coincubation.

To study the effect of infection on DC stimulatory capacity, matDC and infDC were simultaneously coincubated with allogeneic CFSE-labeled $CD4^+$ T cells in the presence of anti-CD3 beads, and after 3 days T cell proliferation was assessed by flow cytometry. Significant reduction in T cell proliferation (up to 60%) was observed when T cells were coincubated with infDC, pointing out that infDC display an impaired ability to stimulate $CD4^+$ T cells compared with matDC (Fig. 2*B*). Reduced T cell proliferation was accompanied by reduced IFN-γ production (data not shown). In the second set of experiments, DC were preincubated for 24 h (to allow induction of inhibitory mechanisms after infection) and prior T cells were added for a coculture (Fig. 2*C*). Under these conditions T cell proliferation was also significantly reduced (up to 75%) in the presence of infDC (Fig. 2*C*), and this reduction was even more profound as in a direct coculture (Fig. 2*B*).

Subsequently, we determined whether infected DC can suppress the proliferation of activated T cells when provided with a strong stimulatory signal (anti-CD3 plus anti-CD28 beads). For this purpose, DC were added to T cell/bead cocultures at the onset of stimulation (Fig. 2*D*). T cells strongly proliferated when stimulated by anti-CD3/anti-CD28 beads, and addition of matDC did not significantly increase T cell proliferation (Fig. 2*D*). In contrast, proliferation of CD3/CD28-activated T cells was significantly lower when cocultured with infected DC (Fig. 2*D*). The suppression of CD3/CD28-induced T cell proliferation was even more evident when the stimulus was suboptimal (1:10 ratio of beads/T cells, Fig. 2*D*). Interestingly, when this assay was performed in a transwell system, where DC were separated from T cell/bead cocultures by a 0.4-μm polycarbonate membrane, the difference between matDC and infDC was substantially less prominent (~10%, data not shown).

Timing of interaction between DC and T cells has an impact on T cell activation (29). Therefore, in the next set of experiments we studied whether pretreatment of T cells with a stimulatory signal (anti-CD3/anti-CD28 beads) for 24 h prior to MLR would have an impact on the suppressive effect of infDC (Fig. 2*E*). In contrast to the experiments presented in Fig. 2*D*, addition of infDC to prestimulated T cells did not alter the proliferation rate of the latter, even when the CD3/CD28 stimulus was suboptimal (Fig. 2*E*). These data indicate that infDC cannot exert inhibitory effects upon previously activated T cells. Altogether, the outcome of encounter between T cells and infDC depends on the timing and T cell preactivation status.

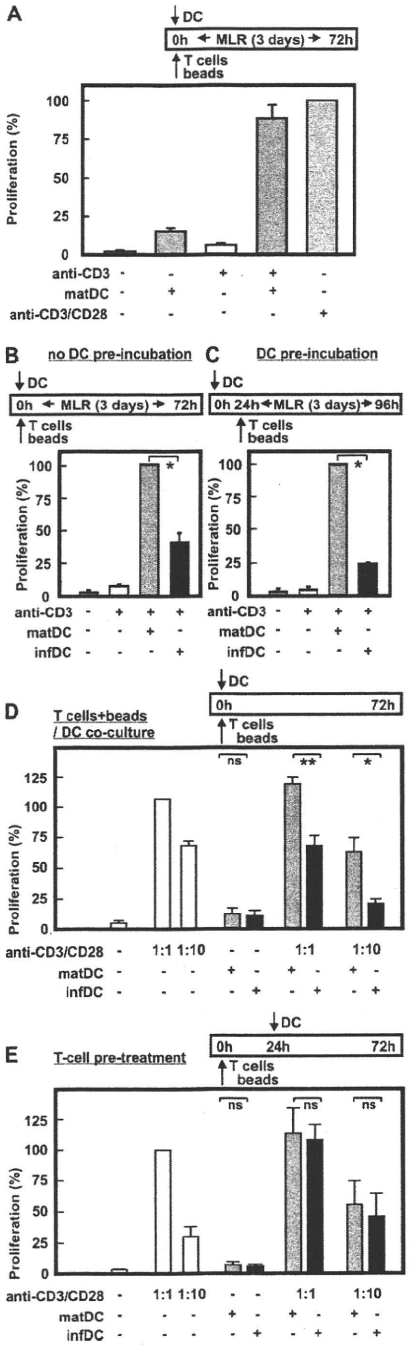

FIGURE 2. DC infected with *L.m.* inhibit T cell proliferation. Immature DC were either infected with *L.m.* (infDC) or stimulated with TNF (matDC). Allogeneic CFSE-labeled $CD4^+$ T cells were coincubated with DC at a ratio of 10:1 (T cells to DC), and beads, coated with either anti-CD3 mAb (anti-CD3) or anti-CD3 and anti-CD28 mAbs (anti-CD3/CD28), were added at different ratios. Asterisks highlight the statistically significant differences; ns, not significant. *A*, Mature DC were cocultured with T cells and anti-CD3 or anti-CD3/CD28 beads (beads/T cell ratio 1:1). After 3 days of coculture, T cell proliferation was assessed by flow cytometry. In the diagram, percentages of proliferating T cells of three independent experiments (relative to the simulation with anti-CD3/CD28 beads alone, taken as 100%; mean ± SD) are shown. *B*, Mature DC or infected DC were extensively washed and cocultured with T cells and anti-CD3 beads without preincubation (beads/T cell ratio 1:1). After 3 days of coculture T cell proliferation was assessed by flow cytometry. Percentages of proliferating T cells of three independent experiments (relative to the simulation with matDC, taken as 100%; mean ± SD) are shown. *, $p < 0.005$. *C*, Mature DC or infected DC were preincubated at 1×10^5/ml in 96-well plates. After 24 h, T cells and anti-CD3 beads were added (beads/T cell ratio 1:1), and after further 3 days of culture T cell proliferation was assessed by flow cytometry. Percentages of proliferating T cells of three independent experiments (relative to the simulation with matDC, taken as 100%; mean ± SD) are shown. *, $p < 0.0001$. *D*, Allogeneic CFSE-labeled $CD4^+$ T cells were coincubated with anti-CD3 and anti-CD28 beads (beads/T cells ratio 1:1 for optimal simulation and 1:10 for suboptimal stimulation; light gray bars). Simultaneously, mature DC stimulated with TNF (matDC, dark gray bars) or DC infected with *L.m.* (infDC, black bars) were added to T cells at a ratio of 1:10 (DC/T cells). As a control, T cells were left unstimulated or stimulated with DC alone. Three days upon the onset of T cell culture, T cell proliferation was assessed by flow cytometry. In the diagram, percentages of proliferating T cells of three independent experiments (relative to the optimal simulation with anti-CD3/CD28 beads (ratio 1:1) alone, taken as 100%; mean ± SD) are shown. *, $p < 0.05$ and **, $p < 0.005$. *E*, Same as *D*, except that DC were added only 24 h after the onset of T cell/beads coculture.

Next we assessed whether infDC-derived soluble factors are sufficient to suppress the CD3/CD28-activated T cell proliferation (Fig. 3). For this purpose, CD3/CD28-activated T cells were incubated with a concentration range of DC-derived supernatants (0–100%) or with kynurenine, IL-10, and PGE_2; the latter assay was also performed in a tryptophan-free medium. Addition of infDC-derived supernatants to activated T cells resulted in a significant suppression of T cell proliferation, starting from 20% dilution, when compared with the same amount of matDC-derived supernatants (Fig. 3*A*).

Furthermore, addition of kynurenine to CD3/CD28-activated T cells was sufficient to suppress the T cell proliferation, and this effect was even more profound when the assay was performed in a tryptophan-free medium (Fig. 3*B*). Combination of low tryptophan and kynurenine (as a model of IDO enzymatic activity), as well as addition of IL-10 or PGE_2, led to a comparable and significant reduction of CD3/CD28-induced T cell proliferation (Fig. 3*B*).

While inhibitory functions of IL-10 (30), IDO (14), and COX-2-mediated PGE_2 (27) have been well established (Fig. 3*B*), the role of cell-surface CD25 and soluble CD25 is less clear (26, 31). IL-2-dependent CTLL-2 cells and heat-killed *L.m.* were used to address this question. Heat-killed *L.m.* induce similar amounts of CD25 in infDC (data not shown) but no IDO and COX-2 (10), so it was chosen to study the function of CD25 expression on infected DC. As shown in Fig. 3*C*, the number of viable CTLL-2 cells was significantly reduced in cultures incubated with supernatants from infDC in comparison to matDC. As a consequence, an increase of dead CTLL-2 cells in supernatants from infDC was observed (Fig. 3*D*). This was associated with a 30% reduction of IL-2 in culture supernatants as measured by ELISA (data not shown).

To determine the impact of individual inhibitory mechanisms, $CD4^+$ T cells were cocultured with infDC together with IL-2 (as a CD25 antagonist) and inhibitors against COX-2, IL-10, or IDO. Blockade of IDO, COX-2, and IL-10 individually did not significantly change T cell proliferation in presence of infDC, and IL-2 was also without effect (Fig. 3*E*). Only with inhibiting COX-2, IL-10, and IDO in the presence of IL-2 was an increase in T cell proliferation detected (Fig. 3*E*). Overall, these data indicate that multiple inhibitory mechanisms that are capable to turn infDC into regulatory DC are induced during infection.

Regulatory phenotype of infected DC is controlled predominantly by TNF

In addition to IFNs (14), we have recently revealed TNF as a potent inducer of the inhibitory molecule IDO (10). Here, we assessed the role of IFN-γ, TNF, and TNF-RI and TNF-RII on the